Contrib Mineral Petrol (2006) 152:421–441
DOI 10.1007/s00410-006-0120-5

ORIGINAL PAPER

Ultrahigh pressure metamorphic rocks from the Chinese Continental Scientific Drilling Project: I. Petrology and geochemistry of the main hole (0–2,050 m)

Zeming Zhang · Yilin Xiao · Jochen Hoefs · J. G. Liou · Klaus Simon

Received: 5 May 2006 / Accepted: 26 May 2006 / Published online: 18 July 2006

Abstract The main hole (MH) of the Chinese Continental Scientific Drilling Project (CCSD) in southern Sulu has penetrated into an ultrahigh-pressure (UHP) metamorphic rock slice which consists of orthogneiss, paragneiss, eclogite, ultramafic rock and minor schist. Recovered eclogites have a UHP metamorphic mineral assemblage of garnet + omphacite + rutile ± phengite ± kyanite ± coesite ± epidote. Ultramafic rocks contain garnet + olivine + clinopyroxene + orthopyroxene ± Ti-clinohumite ± phlogopite. Gneisses and schists contain an amphibolite-facies paragenesis, but their zircons have coesite, garnet, omphacite (or jadeite) and phengite inclusions, indicating that eclogites and gneisses have been subjected to in situ UHP metamorphism. Using available geothermobarometers, *P–T* estimates of 3.1–4.4 GPa and 678–816°C for eclogites were obtained. If surface outcrops and neighboring shallow drill holes are considered together, we suggest that a huge supracrustal rock slab (> 50 km long × 100 km wide × 5 km deep) was subducted to a depth > 100 km and then exhumed to the surface. The depth interval (0–2,050 m) of the CCSD-MH can be divided into six lithological units. Unit 1 consists of alternating layers of quartz-rich and rutile-rich eclogites, with thin interlayers of gneiss and schist. Eclogites of unit 1 are characterized by Nb, Ta, Sr and Ti depletions, low Mg number and general LREE enrichment. Unit 2 comprises rutile- and ilmenite-rich eclogite and minor ''normal'' eclogite and is characterized by high TiO_2, total Fe, V, Co and Sr, and very low SiO_2, alkali, Zr, Ba, Nb, Ta and total REE contents, and LREE-depleted REE patterns with slightly positive Eu anomalies. Unit 3 contains ultramafic rock and minor MgO-rich eclogite. Protoliths of UHP rocks from units 1, 2 and 3 represent a layered mafic to ultramafic intrusion at crustal depth. Units 4 and 6 consist of interlayered eclogite and paragneiss; the eclogites are characterized by Th, U, Nb, Ta and Ti depletion and K enrichment and LREE-enriched REE patterns. Paragneisses show Nb, Ta, Sr and Ti depletions and LREE-enriched REE patterns occasionally with slightly negative Eu anomalies, indicating that their protoliths represent metamorphic supracrustal series. Unit 5 consists mainly of orthogneisses, showing distinct Nb, Ta, Sr and Ti depletions, and LREE-enriched REE patterns with pronounced negative Eu anomalies, suggesting granitic protoliths. In conclusion it is proposed that the southern Sulu UHP belt consists of a series of meta-supracrustal rocks, a layered mafic–ultramafic complex and granites.

Communicated by T.L. Grove

Z. Zhang (✉)
Institute of Geology, Chinese Academy of Geological Sciences, 26 Baiwanzhuang Road, Beijing 100037, China
e-mail: zzm@ccsd.org.cn

Y. Xiao · J. Hoefs · K. Simon
Geowissenschaftliches Zentrum der Universität Göttingen, Goldschmittstrasse 1, 37077 Göttingen, Germany

J. G. Liou
Department of Geological and Environmental Sciences, Stanford University, Stanford, CA 94305, USA

Introduction

The Dabie-Sulu orogen was formed by the collision of North China and the Yangtze plate. It is probably one of the most investigated collisional orogens in the

world due to the widespread occurrences of coesite-bearing UHP metamorphic rocks (Liou et al. 1995; Cong et al. 1996; You et al. 1996; Wallis et al. 1999), which record a complete geodynamic cycle and constrain the mechanisms of continental crust subduction to and exhumation from depths greater than 100 km. Previous studies have provided constraints on the UHP event in the Dabie-Sulu area, but could deal only with sporadic outcrop samples (e.g., Hirajima et al. 1990; Enami et al. 1993; Zhang et al. 1994, 1995a, 2000a) and shallow holes (e.g., Yang and Jahn 2000; Yang 2003; Zhang et al. 2000b; Liu et al. 2001). Petrochemical investigations of spatially continuously exposed UHP rocks have not been possible so far.

The drill site of the CCSD is located near Maobei village (N34° 25′, E118° 40′), about 17 km southwest of Donghai in the southern segment of the Sulu UHP terrane (Fig. 1). Major goals of the CCSD, as outlined by Xu et al. (1998), include (1) to reveal the crustal structure of convergent plate boundaries, (2) to provide constraints on crust–mantle interactions and mantle behavior during deep subduction of continental crust, and (3) to investigate fluid evolution during UHP metamorphism. The CCSD-MH was completed at its final depth of 5,158 m in March 2005. In this paper, we report petrochemical data of core samples, collected at 1–4 m intervals from 100 to 2,050 m of the CCSD-MH, and discuss the nature of protoliths, metamorphic *P–T* conditions of the UHP rocks and the compositional relationship between the minerals and their host rock. We demonstrate that huge volumes of supracrustal rocks have been subjected to in situ UHP metamorphism as a coherent terrain, as has already been shown by previous investigations of surface and drill hole samples (e.g., Zhang et al. 1994, 1995a, b, 2000b, 2003; Ya et al. 2000; Liu et al. 2001, 2004, 2005a). Moreover, *P–T* estimates using various geothermobarometers indicate that UHP rocks from the main hole might be formed under different peak-metamorphic conditions. We suggest that some chemical compositions of UHP minerals were controlled mainly by their protoliths rather than metamorphic *P–T* conditions. Mineral abbreviations used in this paper are after Kretz (-1983) except: Ae = aegirine, Amp = amphibole, Cel = celadonite, Coe = coesite and Phn = phengite. Rock abbreviations: Ec = eclogite, Nor-Ec = normal eclogite, Mg-Ec, Qtz-Ec, Phn-Ec, Rt-Ec and Rt-Ilm Ec are MgO-, quartz-, phengite-, rutile- and rutile- and ilmenite-rich eclogite, respectively, Ogn = Orthogneiss, Pgn = paragneiss and Sch = schist.

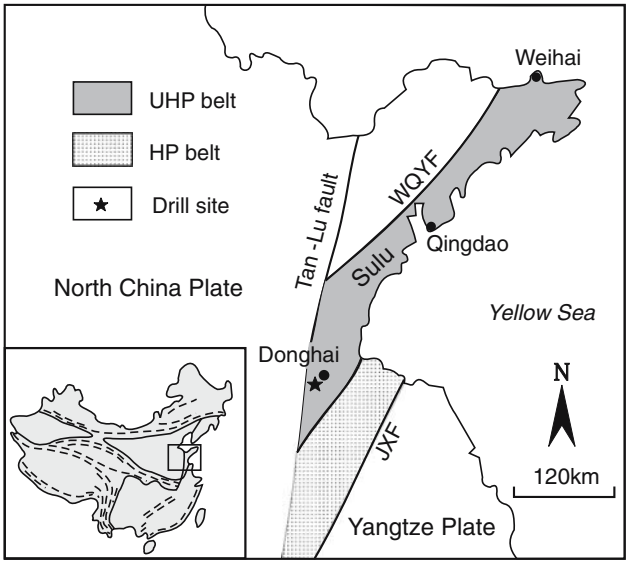

Fig. 1 Simplified geological map of the southern Sulu UHP metamorphic belt, showing the location of the CCSD-MH by a *star* symbol. *JXF* Jiashan-Xiangshui fault, *WQYF* Wulian-Qingdao-Yantai fault

Analytical methods

For whole rock chemical analysis, about 500 g core material for each sample was crushed to about 60 mesh in a steel jaw crusher. About 60 g was powdered in an agate ring mill to less than 200 mesh. All samples were analyzed in the National Geological Analysis Center of China, Beijing. Major elements of bulk rock samples were determined by XRF (Rigaku-3080). The analytical uncertainty is < 0.5%. Trace elements Zr, Nb, V, Cr, Sr, Ba, Zn, Ni, Rb and Y were determined using another XRF instrument (Rigaku-2100). The analytical uncertainties are < 5% for Ba and < 3% for other elements. Other trace elements and rare earth elements (REE) were analyzed by ICP-MS (TJA-PQ-ExCell). The analytical uncertainties are 1–5% at abundances > 1 ppm and 5–10% at abundances < 1 ppm. To test the reliability of the results, repeated analyses of about 30 samples were independently carried out at the Geoscience Centre of Göttingen University in Germany and at the Department of Earth Science of Rice University in the USA. Results from the three laboratories are consistent within analytical errors.

Mineral compositions were determined by electron-microprobe analysis using a JXA-8900RL Jeol Superprobe equipped with WDS/EDS combined micro-analyzer at the Geoscience Centre of Göttingen University. Analyses were performed on polished sections at 15 kV accelerating voltage, 12 nA beam current and usually 5 μm probe diameter. Standards

include silicates and pure oxides. Raw data were calculated by the CITZAF method of Armstrong (1991). Laser Raman analysis of mineral inclusion in zircon was performed on the RENISHAW Raman spectrometer (RM100) at the Institute of Geology, CAGS, China.

Lithological profiles of the CCSD-MH (0–2,050 m)

From 0 to 100 m of the CCSD-MH only rock cuttings were collected. The section from 100 to 2,050 m has a core recovery of ~ 80%. Eclogites and orthogneisses are the principal lithological types (Fig. 2). Eclogites have a total thickness of about 1,200 m and mainly occur at depth intervals of 100–1,100 m and 1,600–2,050 m; orthogneisses mainly occur between 1,100 and 1,600 m; other rock types comprise paragneiss, ultramafic rock and, rarely, schist and quartzite. According to their spatial distribution, occurrence, rock association and compositional variation, the rocks from 100 to 2,050 m can be divided into six lithological units (Fig. 2). With increasing depths, they are: unit 1 (from 100 to 530 m) consists mainly of quartz-rich eclogite, intercalated layers of rutile-rich eclogite and thin layers of paragneiss; unit 2 (from 530 to 600 m) is composed mainly of rutile- and ilmenite-rich eclogites; unit 3 (from 600 to 680 m) consists of ultramafic rock with minor eclogites and garnet clinopyroxenite as thin layers and blocks; unit 4 (from 680 to 1,160 m) is composed mainly of interlayered paragneiss, eclogite and retrograded eclogite (amphibolite) and a thin layer of ultramafic rock; unit 5 (from 1,160 to 1,600 m) consists mainly of orthogneiss with thin layers of par-

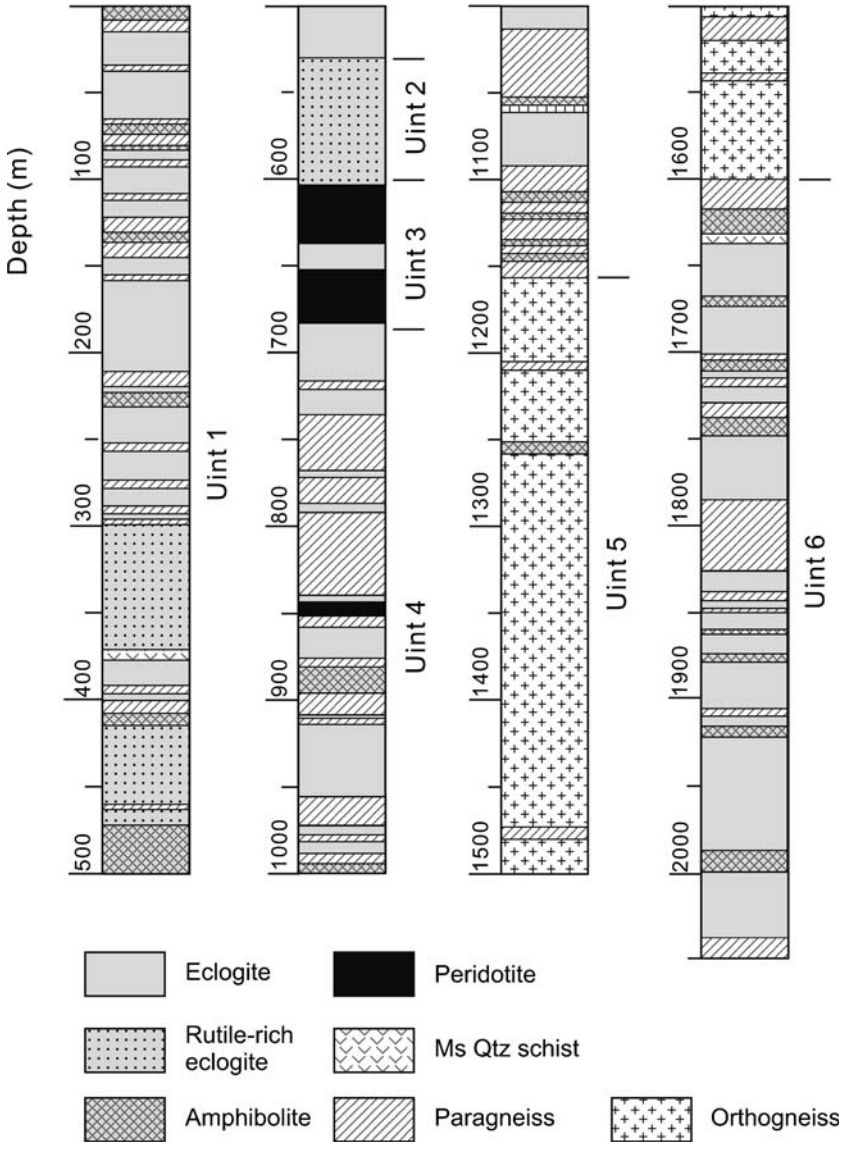

Fig. 2 Lithological profile of the CCSD-MH (0–2,050 m)

agneiss and amphibolite; and unit 6 (from 1,600 to 2,050 m) consists mainly of eclogite with minor paragneisses occurring as interlayer in the middle part of the unit.

Petrography

Eclogite

Eclogites have a UHP metamorphic mineral assemblage of garnet + omphacite + rutile + zircon ± phengite ± kyanite ± coesite (or quartz) ± epidote. Based on mineral modal abundances, eclogites can be divided into five types. (1) ''Normal'' eclogite mainly in units 1, 4 and 6 consists of garnet and omphacite with minor amounts of other phases (e.g., phengite, epidote, quartz and rutile). (2) Quartz-rich eclogite in units 1 and 4 contains quartz up to 10–20 vol.%. (3) Phengite- and/or kyanite-rich eclogites mainly occur in units 4 and 6; they are characterized by high contents of phengite + kyanite > 10 vol.% (Fig. 3a). (4) Rutile- and/or ilmenite-rich eclogites in units 1 and 2 have a characteristic mineral assemblage of garnet + omphacite + rutile ± apatite ± limonite (Fig. 3b). (5) MgO-rich eclogites occur as lenses or blocks within ultramafic rock of unit 3, which can be distinguished from the other types of eclogites by their high MgO content and simple mineral assemblage (Grt + Omp + Rt).

Generally, eclogites have been subjected to various degrees of amphibolite-facies retrogression. Omphacite is replaced by amphibole and sodic plagioclase symplectite, and garnet by amphibole and plagioclase

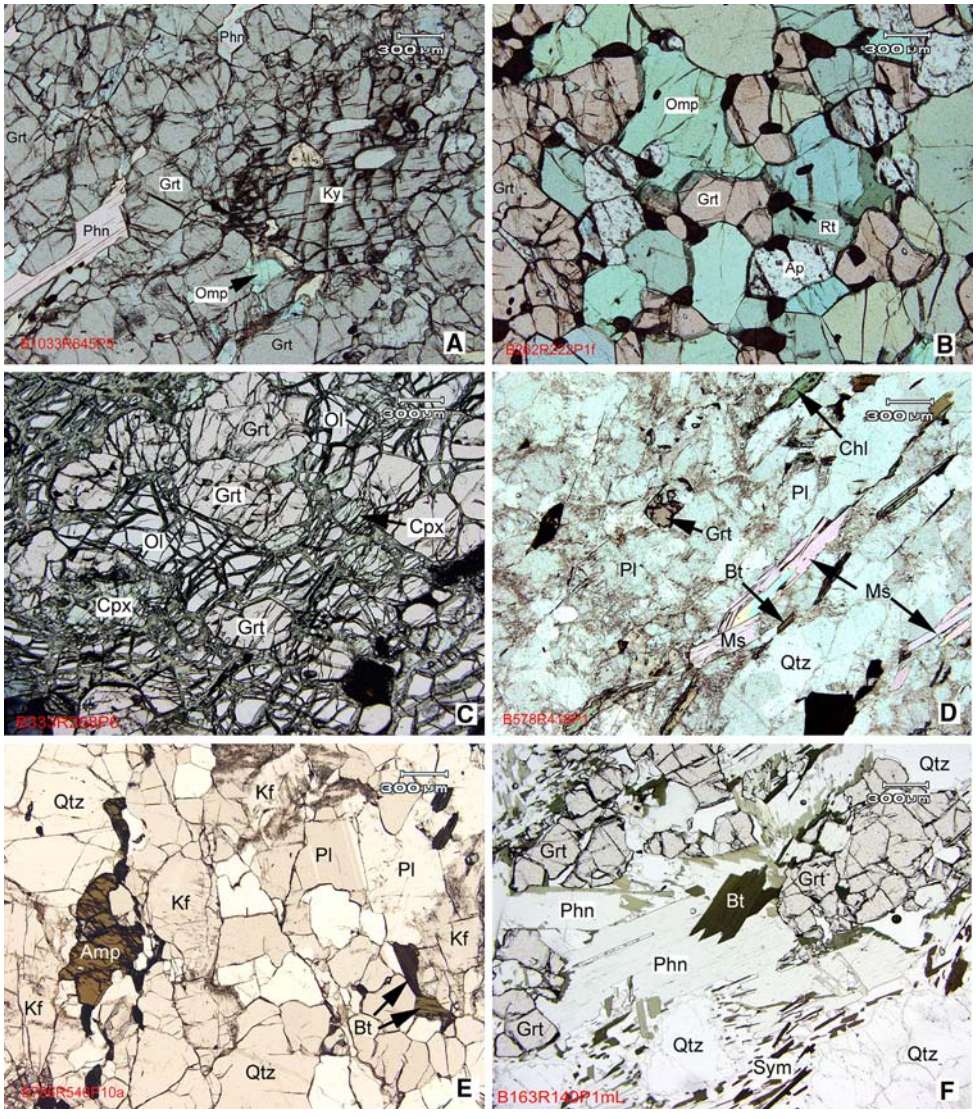

Fig. 3 Microphotographs of eclogites. **a** Phn eclogite (B1033R645P5, 1,964 m), containing garnet, omphacite, phengite, kyanite and quartz. Plane light. **b** Rt eclogite (B262R222P1f, 533 m), containing abundant rutile and apatite and minor amphibole. Plane light. **c** Garnet peridotite (B333R268P6, 652 m), containing olivine, garnet and clinopyroxene, and secondary serpentine and magnetite. Plane light. **d** Paragneiss (B578R418P1, 1,050 m), consisting of plagioclase, quartz, K-feldspar, muscovite, biotite, garnet and pyrite. Some biotites are replaced by chlorite. Plane light. **e** Orthogneiss (B786R546P10a, 1,504 m), consisting of K-feldspar, plagioclase, quartz, amphibole and biotite. Plane light. **f** Garnet-phengite-quartz schist (B163R140P1mL, 371 m). Phengites are rimmed by biotite and plagioclase symplectitic corona. Plane light

symplectite. Some eclogites have been completely transformed to amphibolite or epidote–biotite schist. Inclusions of polycrystalline quartz pseudomorph after coesite are common in garnet and omphacite. By laser Raman analysis, coesite, garnet, omphacite and phengite are recognized as inclusions in zircons from fresh and retrograde eclogites (Fig. 4a), indicating that all eclogites have been subjected to UHP metamorphism (also see Liu et al. 2004; Zhang et al. 2006).

Ultramafic rock

Ultramafic rocks, including garnet peridotite (Fig. 3c) and garnet pyroxenite, occur in unit 3 and consist of garnet, olivine, clinopyroxene and orthopyroxene, with or without minor Ti-clinohumite and phlogopite. In many cores, ultramafic rocks contain blocks of eclogite. Some garnet pyroxenites show well-developed mineral lineation defined by elongated clinopyroxene and garnet. Most ultramafic rocks exhibit variable degrees of hydrous alteration as indicated by partial to complete serpentinization.

Gneiss and schist

Paragneiss includes epidote–biotite gneiss, garnet–biotite–muscovite gneiss (Fig. 3d) and garnet–muscovite gneiss. They occur as layers intercalated with eclogites, or as thin layers, bands or stripes within eclogites in units 1, 4 and 6. They also rarely occur as thin interlayers within orthogneiss in unit 5. The boundary between paragneisses and eclogites is generally sharp, only occasionally transitional.

Orthogneisses, including amphibole–biotite gneiss (Fig. 3e), two-mica gneiss and garnet-two micas gneiss, occur as a meta-granitic body at the depth interval of 1,200–1,600 m (unit 5). In comparison with paragneisses, orthogneisses have lower abundances of ferromagnesian minerals and show only slight foliation or even massive structure.

Schists occur as very thin layers (< 10 cm) within paragneiss and eclogite. Three types of schists may be distinguished according to their mineral assemblages: garnet-white mica quartz schist, garnet two-mica schist (Fig. 3f) and garnet–epidote–biotite quartz schist. Schists have similar mineral assemblages like the paragneisses, but higher contents of mica and quartz.

Paragneiss and orthogneiss have amphibolite-facies mineral assemblages. Plagioclase, K-feldspar, biotite, epidote, amphibole, garnet, muscovite and quartz are the principal phases. However, symplectitic textures of biotite and plagioclase after phengite and of amphibole and plagioclase after omphacite and garnet are recognized in several gneiss samples. Moreover, coesite inclusions are common in zircons from paragneiss, orthogneiss and schist (Fig. 4b–d). Other minerals,

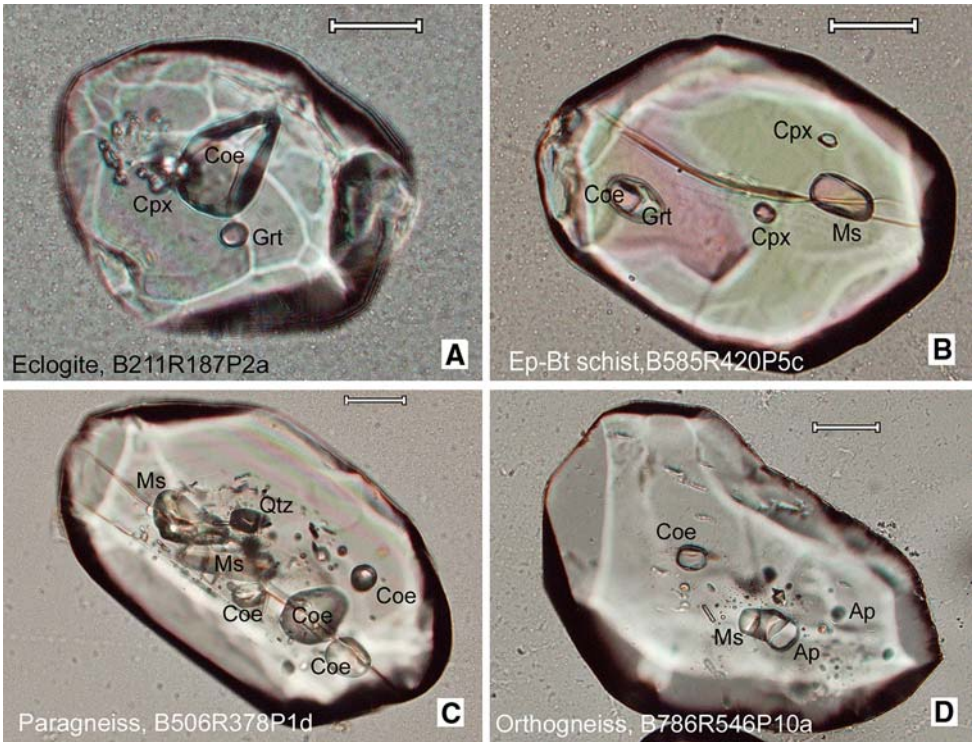

Fig. 4 Microphotographs of zircons and their mineral inclusions (plane light, all scale bars are 30 μm). **a** Eclogitic zircon containing inclusions of coesite, garnet, clinopyroxene and some fine-grained unknown minerals (B211R187P2a, 453 m). **b** Zircon in epidote–biotite schist (B585R420P5c, 1,062 m) containing inclusions of coesite, garnet, clinopyroxene and muscovite. **c** Zircon in paragneiss (B506R378P1d, 930 m) containing inclusions of coesite, muscovite, quartz and some fine-grained unknown minerals. **d** Zircon in orthogneiss (B786R546P10a, 1,504 m) containing inclusions of coesite, muscovite, apatite and some fine-grained unknown minerals

such as phengite, garnet, omphacite (or jadeite), rutile, calcite (or aragonite) and apatite, were also recognized as inclusions in some zircon grains (Liu et al. 2004; Zhang et al. 2006). The occurrence of coesite inclusions strongly suggests that these rocks have been subjected to early UHP metamorphism before amphibolite-facies overprint, consistent with the results on non-mafic rocks from shallow drill holes and surface outcrops (> 50 × 100 km^2) in Donghai (Zhang et al. 2000b; Liu et al. 2001). Based on studies of samples from depths of 2,050–5,158 m, coesite inclusions were frequently recognized in gneissic zircons (Liu et al. 2005a; Zhang et al. 2006). These facts indicate that voluminous supracrustal rocks have been subducted as a coherent continental slab (> 50 × 100 × 5 km^3) to mantle depth.

Mineral chemistry

Representative data of analyzed garnet, clinopyroxene and phengite are listed in Tables 1, 2 and 3 and described in detail as follows. Note that Fe_2O_3 contents of pyroxene and garnet were recalculated by stoichiometric charge balance.

Garnet

Garnets from eclogites show a very wide range of compositions (Fig. 5, Table 1) and vary with their host rock compositions. Garnets with high pyrope contents (> 37%) are present in eclogites within the ultramafic rock. Most almandine-rich garnets occur in Rt- or Ilm-rich eclogites from units 1 and 2. FeO, MgO and Al_2O_3 contents of garnets are positively correlated with those of the whole rocks (Fig. 6a, b), implying that they do not depend on metamorphic conditions. In contrast, CaO contents are not correlated with the whole rocks. Garnets from gneisses and schists contain very low pyrope (2–15%), high grossular (32–52%) and almandine (33–59%) components (Fig. 5). Some garnets contain relatively high spessartine contents (up to 32%) (Table 1) and exhibit retrograde compositional zoning, in which MgO and CaO decreases, and MnO increases from core to rim, indicating an origin of amphibolite-facies metamorphism.

Some garnet porphyroblasts in normal eclogite contain abundant mineral inclusions and show complex growth zonations (Zhang et al. 2005a). The inclusions display a distribution pattern that is related to the compositional variation of the host garnet, with amphibole and epidote inclusions occurring in the inner segment of the garnet and omphacite and quartz inclusions present in the outer segment. Growth zonations and mineral inclusion distribution patterns suggest a typical two-stage growth formation, i.e. (1) an early stage of prograde growth from core to mantle with a decrease of Fe/Mg ratios, suggesting an increase in metamorphic temperature, and (2) a late stage of retrograde growth with distinct increases of Fe/Mg ratios from mantle to rim, implying a temperature and pressure decrease. Similar complex garnet growth zoning has been reported for UHP eclogites from Junan localities (Enami and Nagasaki 2000) and

Table 1 Representative microprobe analysis of garnet in the UHP rocks from the drill hole

Number	1	2	3	4	5	6	7	8	9	10	11	12	13
Depth (m)	102	115	574	613	685	1,003	1,964	902	930	1,050	1,109	282	371
Unit	1	1	2	3	3	4	6	4	4	4	4	1	1
Rock	Qtz-Ec	Qtz-Ec	Rt-Ec	Mg-Ec	Mg-Ec	Nor-Ec	Phn-Ec	Pgn	Pgn	Pgn	Pgn	Sch	Sch
SiO_2	38.19	37.58	38.56	40.53	40.30	39.13	40.44	38.14	37.58	37.38	37.49	38.32	37.83
TiO_2	0.028	0.043	0.13	0.000	0.020	0.028	0.023	0.02	0.05	0.07	0.12	0.00	0.04
Al_2O_3	21.45	20.88	20.60	22.64	21.64	21.65	22.70	20.85	20.74	19.56	19.97	21.64	21.45
Cr_2O_3	0.00	0.00	0.00	0.39	0.06	0.00	0.00	0.02	0.00	0.00	0.02	0.01	0.02
FeO	26.59	27.69	24.49	17.29	16.96	21.35	15.54	21.32	21.87	21.49	15.87	25.90	25.88
MnO	1.08	1.72	0.49	0.47	0.38	0.49	0.29	1.39	4.54	9.68	14.03	0.94	1.18
MgO	3.69	1.93	5.20	15.69	15.45	8.63	11.91	1.51	0.68	0.39	0.99	3.86	3.18
CaO	9.51	9.94	10.54	3.78	4.47	8.85	9.35	16.11	14.16	11.32	11.00	9.95	10.81
Na_2O	0.06	0.07	0.04	0.02	0.00	0.04	0.03	0.03	0.06	0.01	0.01	0.03	0.03
Total	100.62	99.86	100.05	100.81	99.27	100.17	100.28	99.42	99.69	99.92	99.51	100.65	100.42
Prp	0.145	0.077	0.201	0.578	0.571	0.330	0.440	0.059	0.027	0.016	0.039	0.151	0.126
Grs	0.268	0.285	0.293	0.100	0.119	0.243	0.248	0.454	0.405	0.324	0.314	0.279	0.307
Alm	0.563	0.599	0.495	0.313	0.302	0.417	0.306	0.456	0.465	0.441	0.330	0.550	0.541
Sps	0.024	0.039	0.011	0.010	0.008	0.011	0.006	0.031	0.103	0.219	0.317	0.021	0.026

Sample number: *1* B1R1P1a, *2* B8R12P1a, *3* B287R235p1o, *4* B308R253P7-1, *5* B353R283P1d, *6* B552R399P11, *7* B1033R645P5, *8* B488R369P1h, *9* B506R378P1d, *10* B578R418P1, *11* B616R436P1aL, *12* B107R98P6d, *13* B163R140P1m

Table 2 Representative microprobe analysis of clinopyroxene in the UHP rocks from the drill hole

Number	1	2	3	4	5	6	7	8	9	10	11	12
Depth (m)	102	115	347	532	533	576	613	685	688	731	1,003	1,964
Unit	1	1	1	2	2	3	3	3	4	4	4	6
Rock	Qtz-Ec	Qtz-Ec	Rt-Ec	Rt-Ec	Rt-Ec	Rt-Ec	Mg-Ec	Mg-Ec	Phn-Ec	Nor-Ec	Nor-Ec	Phn-Ec
SiO_2	57.22	57.14	55.86	53.70	55.78	54.69	54.56	54.88	55.75	56.31	55.55	56.27
TiO_2	0.05	0.08	0.08	0.05	0.07	0.07	0.00	0.00	0.03	0.07	0.09	0.03
Al_2O_3	16.28	16.63	10.94	5.15	8.61	5.46	1.19	0.29	8.25	11.19	10.73	10.25
Cr_2O_3	0.02	0.00	0.03	0.00	0.03	0.04	0.16	0.00	0.01	0.02	0.02	0.00
FeO	5.26	7.02	5.92	11.59	7.82	9.97	4.07	2.32	1.66	2.50	7.61	1.91
MnO	0.05	0.06	0.00	0.04	0.02	0.00	0.06	0.03	0.02	0.00	0.06	0.00
MgO	3.90	2.37	7.03	7.99	8.00	9.00	16.24	17.64	12.09	9.11	6.51	10.20
CaO	6.41	4.46	10.72	14.33	12.20	14.89	21.94	23.57	17.62	13.57	10.40	14.71
Na_2O	10.70	11.77	7.85	5.79	7.00	5.62	1.50	0.37	4.62	6.79	8.45	5.73
K_2O	0.00	0.00	0.01	0.02	0.00	0.01	0.01	0.01	0.00	0.00	0.01	0.00
Total	99.91	99.53	98.46	98.65	99.55	99.74	99.74	99.19	100.07	99.56	99.42	99.14
Jd	0.69	0.71	0.48	0.23	0.38	0.24	0.05	0.01	0.35	0.48	0.46	0.45
Acm	0.06	0.12	0.09	0.21	0.13	0.17	0.08	0.01	0.00	0.00	0.15	0.00
Di	0.17	0.10	0.34	0.43	0.39	0.47	0.84	0.92	0.63	0.46	0.33	0.53
Hd	0.08	0.07	0.09	0.15	0.10	0.13	0.05	0.05	0.05	0.07	0.08	0.06

Sample number: *1* B1R1P1a, *2* B8R12P1a, *3* B149R127P7, *4* B261R222P1a, *5* B262R222P1f, *6* B289R235P1m, *7* B308R253P7, *8* B353R283P1d, *9* B355R283P1o, *10* B382R300P2aL, *11* B552R399P11, *12* B1033R645P5

Qinglongshan (Zhang et al. 2005b), about 25 and 90 km away from the CCSD drill site, respectively. These findings indicate that garnet porphyroblasts with compositional zonations are common in Sulu UHP eclogites.

Clinopyroxene

Clinopyroxenes from the matrix of eclogites are variable in composition with 23–71% jadeite component and less than 21% aegirine component (Table 2). Clinopyroxene corona of garnet has augite composition (Jd < 9 %) that was formed during amphibolite-facies retrogression. Omphacites in eclogites do not show compositional growth zoning. However, some omphacite crystals display irregular fragments or bands of diffusive zonations. Na_2O, MgO and FeO contents of omphacites show positive correlation with whole rocks (Fig. 6c, d), implying that jadeite contents in omphacites do not depend on metamorphic pressure. On the other hand, CaO and Al_2O_3 of clinopyroxenes are not related to whole-rock compositions.

White mica

White micas in eclogites and as relics in gneisses and schists are characterized by high Si content (3.1–3.6 p.f.u., O = 11), and are phengites (Table 3). Electron microprobe EBS images show that many phengites have diffusive zoning, commonly with a large core of high Si (3.5–3.6) and a narrow and irregular rim of lower Si (3.2–3.3) (Table 3). This indicates that the phengitic high-Si micas formed under UHP metamorphism whereas the low-Si muscovitic rim recrystallized during the early retrogression of UHP rocks. Furthermore, phengite zonations are usually cut by symplectitic coronas consisting of biotite and plagioclase, suggesting that the zonation was formed before amphibolite-facies retrogression. Chemical compositions of phengites are not controlled by their host rock compositions. SiO_2 contents of phengites probably reflect metamorphic pressures.

Geochemical characteristics of whole rock

Major elements

Whole-rock samples, including 452 eclogites, some orthogneisses, paragneisses and ultramafic rocks, were analyzed for major and trace elements. But data from ultramafic rocks are not shown in this paper as we have no permission for publishing these data. A few representative analyses are listed in Table 4. Changes of major and trace elements with depth are shown in Figs. 7 and 8. Eclogites cover a wide compositional range from peridotgabbro to diorite, but gabbros and gabbroic diorites are dominant according to the chemical classification and nomenclature of plutonic rocks (Middlemost 1994) (Fig. 9). Rt eclogites plot mainly in the areas of gabbro, peridotgabbro and foidolite; some Rt- and Ilm-rich eclogites mainly from unit 2 plot outside of the peridotgabbro area due to their low SiO_2 contents (as low as 40%). Qtz eclogites

Table 3 Representative microprobe analysis of phengite in the UHP rocks from the drill hole

Number	1	2	3	4	5	6		7	8	9	10	11	12	13	14	15		16
Depth (m)	102	115	688	1,003	1,964	270		754	901	930	1,050	1,109	1,183	1,732	282	278		371
Unit	1	1	4	4	6	1		4	4	4	4	4	5	6	1	1		1
Rock	Qtz-Ec	Qtz-Ec	Phn-Ec	Nor-Ec	Phn-Ec	Pgn		Pgn	Pgn	Pgn	Pgn	Pgn	Pgn	Pgn	Pgn	Sch		Sch
Location						Rim	Core									Rim	Core	
SiO_2	52.07	50.92	53.07	51.42	52.42	45.87	51.18	45.16	45.97	46.48	45.21	49.15	45.91	47.53	47.97	48.48	52.05	52.18
TiO_2	0.45	0.59	0.30	0.28	0.27	0.84	0.52	0.04	0.38	0.74	1.21	0.49	0.27	0.62	0.51	0.49	0.51	0.46
Al_2O_3	23.40	23.33	23.50	23.68	23.81	27.60	22.83	27.89	27.27	26.70	27.40	25.52	25.88	25.54	27.45	25.12	23.18	22.23
Cr_2O_3	0.04	0.00	0.02	0.05	0.04	0.02	0.01	0.03	0.02	0.01	0.03	0.00	0.00	0.01	0.00	0.00	0.02	0.00
FeO	2.99	3.86	0.69	3.01	1.05	5.34	4.31	7.62	6.58	5.84	6.82	4.37	7.36	6.40	4.21	5.91	3.89	3.49
MnO	0.03	0.00	0.00	0.02	0.02	0.07	0.12	0.08	0.07	0.06	0.07	0.10	0.06	0.05	0.04	0.06	0.02	0.05
MgO	4.15	3.65	5.34	4.42	4.99	1.85	3.75	1.57	1.74	1.97	1.40	2.87	1.93	2.19	2.56	2.50	3.88	4.54
CaO	0.00	0.00	0.00	0.01	0.00	0.00	0.00	0.00	0.02	0.01	0.00	0.01	0.00	0.07	0.00	0.00	0.00	0.00
Na_2O	0.28	0.36	0.07	0.21	0.31	0.33	0.15	0.17	0.24	0.30	0.27	0.25	0.10	0.26	0.23	0.24	0.16	0.07
K_2O	10.66	10.80	11.25	10.81	10.60	10.67	10.75	10.84	10.90	10.60	10.71	10.91	11.09	10.70	10.65	11.04	10.75	10.87
Total	94.13	93.51	94.27	93.93	93.55	92.58	93.62	93.44	93.19	92.72	93.09	93.68	92.63	93.36	93.62	93.84	94.47	93.89

Sample number: *1* B1R1P1a, *2* B8R12P1a, *3* B355R283P1o, *4* B552R399P11, *5* B1033R645P5, *6* B100R92P1dA, *7* B398R312P1j, *8* B488R369P1h, *9* B506R378P1d, *10* B578R418P1, *11* B616R436P1aL, *12* B655R462P1c, *13* B901R599Pgb, *14* B107R98P6d, *15* B105R93P1a, *16* B163R140P1m

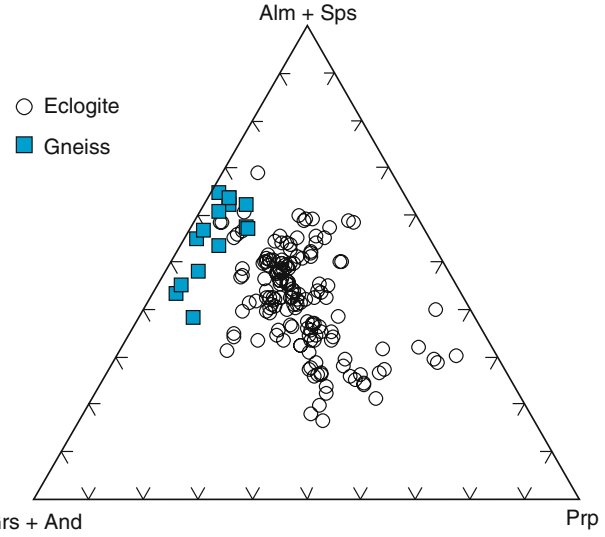

Fig. 5 Compositions of garnets in various UHP rocks

are of diorite and quartz monzonite composition. Normal, phengite and Mg-rich eclogites can be classified as gabbro, gabbroic diorite, monzogabbro or monzodiorite. Most paragneisses range from granodiorite to granite (SiO_2 = 60–75%), whereas orthogneisses lie in the granitic field with higher SiO_2 contents (73–79%).

Eclogites in unit 1 (100–530 m) show the largest variation in SiO_2 from 38 to 61%, TiO_2 (0.7–4.0%, the highest is up to 5.8%) and Al_2O_3 (12–22%) and are characterized by the alternating occurrence of Si-rich Qtz eclogites and Ti-rich Rt eclogites (Fig. 7). Variations of SiO_2 versus MgO, total FeO (TFeO) and TiO_2 show distinct positive correlations, implying a fractional crystallization trend (Fig. 10). Moreover, these rocks have low Mg numbers (mostly < 50%, where the Mg number is $Mg^{2+}/(Mg^{2+} + Fe^{2+}) \times 100$), suggesting that they are not derived from primitive melts. Eclogites from unit 2 (530–600 m) are characterized by high TiO_2 (mostly > 3%) and high TFeO (mostly > 20%) with low SiO_2 (< 45%) and alkali (< 2%) contents (Figs. 7, 10). Their chemical characteristics are consistent with Fe–Ti gabbros from layered intrusions (Parsons et al. 1986; Morrison et al. 1986; McBirney 1989; Wiebe 1993; Arnason et al. 1997; Branadriss and Bird 1999) and with metamorphosed Fe–Ti gabbros (Zhang et al. 1995b; You et al. 1996; Cox et al. 1998; Liou et al. 1998). Eclogites from unit 3 (600–680 m) also show wide compositional ranges (Fig. 10). Eclogites occurring as blocks or lenses within ultramafic rocks are characterized by high MgO (mostly > 12%) contents, distinguishing them from all other eclogites, and suggesting a co-genetic origin with the host rock, whereas eclogites occurring as layers within the center

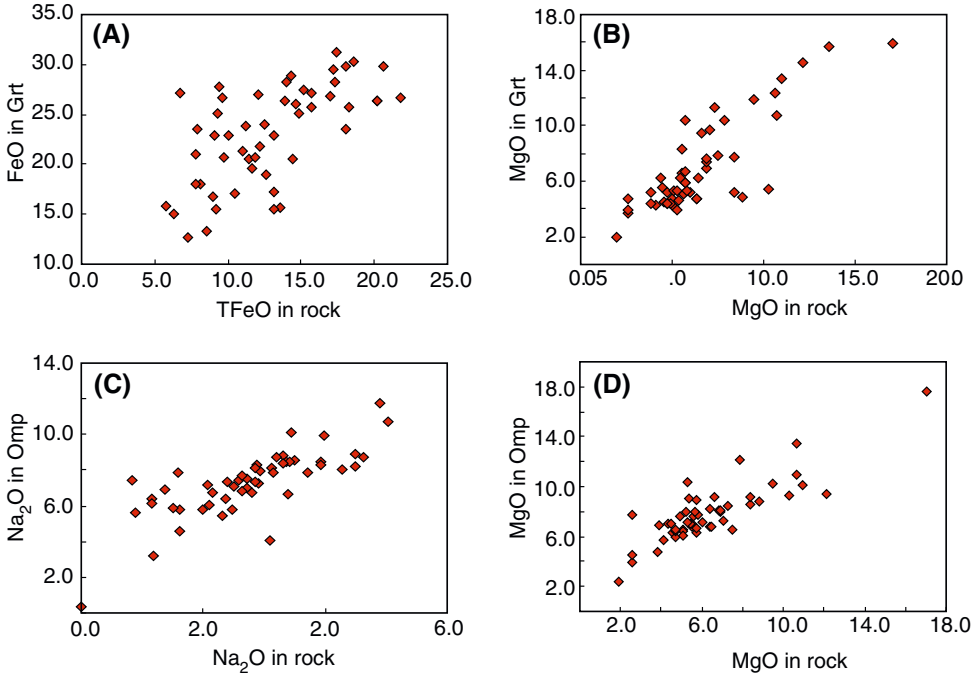

Fig. 6 Oxides correlations between garnet or omphacite and the host rock

of the ultramafic body have compositions which are similar to the normal eclogites from other units. Unit 4 eclogites (680–1,160 m) have compositions close to those from unit 1, but have lower TFeO (mostly < 10%) and TiO_2 (generally around 1%) contents (Fig. 10), showing no fractional crystallization trend. Rarely, eclogites enclosed by orthogneiss from unit 5 (1,160–1,600 m) have high alkali contents (6–8%). Eclogites from unit 6 (1,600–2,050 m) show relatively homogeneous compositions with SiO_2 = 47–50%, TFeO = 8–14% and alkali = 3–5% (Fig. 10; Table 4). In general, all eclogites show comparable but smaller compositional ranges to the continental intrusives from the East Greenland and North Atlantic Province plutonic rocks (http://georoc.mpch-mainz.gwdg.de/georoc/) (Fig. 10).

Trace elements

Trace element abundances of representative samples are listed in Table 4 and are shown in Fig. 8. As shown by Liu et al. (2004, 2005a), both paragneiss and orthogneiss from all units have enriched incompatible element patterns with significant negative Nb, Ta, Sr and Ti anomalies (Fig. 11a, b) and fractionated LREE and flat HREE patterns (Fig. 12a, b); orthogneisses, however, are distinguished from paragneisses by significant negative Eu anomalies. In contrast to orthogneisses, paragneisses and schists have higher Zr, Ba and Sr contents.

A close inspection of the trace element data reveals important compositional differences between eclogites from different units. Eclogites from unit 1 are slightly enriched in incompatible elements compared to ocean island basalts (OIB) but have variable Rb, Ba and Th contents and show distinctly negative Nb, Ta, Sr and Ti anomalies (Fig. 11c), in contrast to any MORB or OIB, whereas their REE patterns are characterized by LREE enrichment and HREE depletion (Fig. 12c), resembling continental basalts (http://georoc.mpch-mainz.gwdg.de/georoc/). Their low Mg numbers (11–54), together with low Cr, Ni and Co concentrations, suggest that they are not primary mantle melts. Eclogites from unit 2 have relatively low mobile element (e.g., Rb, K), low Zr, Ba and Nb contents and total REE abundances, but high V (400–800 ppm), Co (40–80 ppm) and Sc (40–60 ppm) contents (Figs. 8, 11d; Table 4). They are distinguished from all other eclogites by their highly positive Ti and Sr and negative Nb and Ta anomalies (Fig. 11d), i.e., decoupled Ti and V from Nb and Ta. Their REE patterns show flat and depleted LREE and slightly positive Eu anomalies (Fig. 12d). These are typical characteristics of Fe–Ti gabbros in layered mafic to ultramafic intrusions which were formed by extensive fractional crystallization of mafic magma in continental environments (Arnason et al. 1997; Brandriss and Bird 1999; McBirney 1989; Morrison et al. 1986; Wiebe 1993; Parsons et al. 1986). Eclogites from unit 3 vary the most in trace element compositions. Most of them show a depletion in

Table 4 Representative whole-rock major, trace elements and REE compositions of the UHP rocks from the drill hole

Sample	Depth (m)	Unit	Rock	SiO_2	MgO	Al_2O_3	P_2O_5	Na_2O	K_2O	CaO	TiO_2	MnO	Fe_2O_3	FeO	H_2O	CO_2	Total
B1R1P1h	102	1	Qtz-Ec	59.12	2.60	15.23	0.47	5.03	0.63	5.42	1.38	0.35	2.54	7.08	0.40	0.07	100.32
B8R12P1c	115	1	Qtz-Ec	59.47	1.93	13.62	1.09	4.90	1.45	5.24	1.44	0.36	3.44	5.91	0.68	0.24	99.77
B149R127P7	347	1	Rt-Ec	43.34	4.50	14.28	2.83	1.58	0.00	11.24	5.63	0.30	1.72	14.01	0.26	0.04	99.73
B261R222P1a	532	2	Rt-Ec	42.25	5.25	14.37	0.24	2.00	0.02	9.98	4.44	0.36	4.79	15.79	0.42	0.01	99.92
B262R222P1f	533	2	Rt-Ec	42.20	5.68	14.46	2.67	2.72	0.36	10.95	4.18	0.42	3.90	11.84	0.26	0.09	99.73
B289R235P1m	576	2	Rt-Ec	39.16	5.35	18.11	0.01	0.90	0.08	10.34	3.45	0.32	3.53	18.31	0.14	0.01	99.70
B308R254P2	613	3	Mg-Ec	43.30	13.54	17.06	0.53	1.65	0.34	8.50	0.28	0.25	2.76	10.42	1.14	0.31	100.08
B353R283P1g	685	3	Mg-Ec	43.75	17.06	16.85	0.11	0.00	0.00	7.43	0.32	0.23	3.36	10.18	0.54	0.44	100.27
B355R283P1o	688	4	Phn-Ec	45.37	7.89	22.35	0.02	1.62	1.07	12.97	0.53	0.10	1.09	5.16	1.00	0.27	99.45
B382R300P2aL	731	4	Nor-Ec	47.47	8.40	16.59	0.04	2.64	0.09	11.48	1.27	0.19	2.33	9.29	0.48	0.18	100.46
B552R399P11	1,003	4	Nor-Ec	47.77	7.51	16.63	0.38	3.43	1.98	8.24	1.38	0.17	3.82	7.17	1.00	0.25	99.73
B1033R645P5	1,964	6	Phn-Ec	46.90	9.49	17.63	0.18	1.52	2.87	9.11	0.72	0.16	1.51	7.72	0.90	0.88	99.59
B107R98P6k	282	1	Sch	57.02	3.99	15.34	0.42	3.39	2.86	5.78	1.20	0.22	3.12	6.02	0.86	0.09	100.31
B163R140P1mL	371	1	Sch	55.21	3.01	16.49	0.96	2.07	5.10	4.13	2.47	0.30	2.19	6.22	1.74	0.17	100.06
B488R369P1h	902	4	Pgn	64.25	1.78	14.79	0.15	4.10	3.17	3.43	0.78	0.15	2.82	2.75	0.80	0.52	99.49
B506R378P1d	930	4	Pgn	74.36	0.52	13.42	0.05	4.80	1.97	1.19	0.31	0.03	1.03	0.94	0.80	0.13	99.53
B578R418P1	1,050	4	Pgn	66.34	0.62	16.33	0.18	3.29	5.33	0.90	0.86	0.13	2.91	1.06	1.32	0.50	99.78
B616R436P1aL	1,109	4	Pgn	75.95	0.33	12.54	0.06	3.93	2.63	1.39	0.26	0.08	0.70	0.63	0.68	0.46	99.64
B743R516P12L	1,385	5	Ogn	75.09	0.31	11.94	0.06	4.36	4.13	0.74	0.27	0.05	0.79	1.47	0.34	0.55	100.10
B765R532P40	1,447	5	Ogn	75.42	0.26	12.16	0.06	3.73	5.01	0.73	0.24	0.04	1.16	0.95	0.32	0.04	100.12
B786R546P10a	1,504	5	Ogn	76.44	0.07	11.48	0.04	4.53	3.54	0.44	0.13	0.05	1.53	0.92	0.42	0.09	99.68

Sample	Depth (m)	Unit	Rock	Sr	Zr	Ba	V	Zn	Cr	Co	Ni	Cu	Ga	Rb	Nb	Ta	Hf	Pb	Th	U	Sc
B1R1P1h	102	1	Qtz-Ec	226.6	496.9	314.0	54.7	148.4	14.7	10.9	7.9	16.2	21.5	15.9	9.9	0.7	11.8	3.5	2.3	0.4	31.6
B8R12P1c	115	1	Qtz-Ec	412.0	403.0	375.0	48.3	195.1	7.2	9.2	4.6	12.4	22.2	36.9	9.4	0.6	9.5	4.2	4.6	0.7	32.1
B149R127P7	347	1	Rt-Ec	248.9	94.4	56.0	408.8	86.9	4.6	29.7	6.0	24.4	20.4	1.2	4.6	0.3	2.8	5.9	13.9	1.3	42.9
B261R222P1a	532	2	Rt-Ec	91.9	85.0	86.0	505.0	190.0	2.7	44.3	3.1	27.5	17.6	1.6	3.0	0.2	2.7	1.6	0.6	0.2	48.00
B262R222P1f	533	2	Rt-Ec	357.0	51.7	294.0	192.0	165.0	3.1	23.4	3.6	18.5	16.8	8.1	3.6	0.3	1.9	3.7	1.3	0.2	33.20
B289R235Plm	576	2	Rt-Ec	45.6	27.7	43.2	449.0	165.0	269.0	53.3	9.3	149.0	17.0	3.8	0.3	0.0	1.1	2.4	0.0	0.1	41.00
B308R254P2	613	3	Mg-Ec	493.0	44.2	143.0	120.0	71.2	703.0	67.0	328.0	55.3	13.0	9.8	0.5	0.1	1.3	14.2	3.3	0.3	13.60
B353R283Plg	685	3	Mg-Ec	161.0	34.7	3.0	66.0	73.2	300.0	82.4	228.0	20.0	10.6	0.4	0.3	0.0	1.1	1.6	0.3	0.1	16.00
B355R283Plo	688	4	Phn-Ec	773.0	23.5	569.0	86.2	47.5	454.0	36.5	109.0	46.4	13.6	16.4	0.4	0.0	0.8	11.1	1.2	0.2	13.90
B382R300P2aL	731	4	Nor-Ec	72.4	62.4	72.4	279.0	111.0	225.0	52.4	107.0	116.0	19.6	2.5	1.5	0.1	1.9	15.2	0.1	0.1	39.10
B552R399P1l	1003	4	Nor-Ec	155.3	114.0	913.0	227.1	119.7	231.0	53.2	88.4	27.6	18.7	45.9	3.5	0.2	2.4	1.8	0.6	0.1	38.10
B1033R645P5	1964	6	Phn-Ec	103.6	70.9	501.0	134.9	83.4	102.6	63.5	165.7	55.7	14.5	101.1	1.3	0.3	2.1	2.9	0.4	0.1	19.3
B107R98P6k	282	1	Sch	204.3	307.3	769.0	155.6	120.2	32.8	28.0	30.8	16.6	21.9	40.6	7.8	0.6	7.8	2.7	1.6	0.6	24.5
B163R140P1mL	371	1	Sch	213.3	233.0	976.0	105.1	146.6	5.4	12.5	1.3	10.6	23.6	142.3	19.0	1.2	6.4	4.7	2.9	1.0	18.8
B488R369P1h	902	4	Pgn	169.3	227.5	1127.0	85.8	115.9	23.6	11.7	8.8	16.9	19.0	85.7	11.2	0.7	4.9	5.2	2.4	0.6	19.2
B506R378P1d	930	4	Pgn	289.9	266.2	1044.0	12.6	48.4	2.6	1.6	1.2	20.1	17.7	33.0	9.9	0.7	6.3	5.8	13.1	1.5	6.8
B578R418P1	1,050	4	Pgn	173.3	492.0	3432.0	51.8	88.2	3.4	2.8	2.1	12.3	28.1	107.0	22.2	1.0	11.0	4.8	3.4	1.4	9.6
B616R436P1aL	1,109	4	Pgn	240.8	172.6	839.0	28.9	41.1	4.8	2.0	2.7	10.4	20.2	60.2	12.6	0.8	5.2	5.1	11.1	1.6	4.4
B743R516P12L	1,385	5	Ogn	57.8	355.5	445.0	10.4	83.6	4.6	1.7	17.3	15.7	22.0	169.7	18.6	1.2	11.7	20.3	12.4	1.9	3.6
B765R532P40	1,447	5	Ogn	58.3	286.2	707.0	10.0	67.4	3.9	1.6	1.7	4.3	20.7	102.8	14.4	0.8	9.6	13.2	10.1	1.1	3.7
B786R546P10a	1,504	5	Ogn	11.8	432.2	133.0	4.1	143.1	12.0	0.6	6.1	7.4	27.3	128.9	24.4	1.4	19.5	11.0	17.1	2.4	2.2

Table 4 continued

Sample	Depth (m)	Unit	Rock	Y	La	Ce	Pr	Nd	Sm	Eu	Gd	Tb	Dy	Ho	Er	Tm	Yb	Lu
B1R1P1h	102	1	Qtz-Ec	66.1	25.97	62.48	8.92	42.36	10.46	4.02	12.07	2.02	12.7	2.71	8.08	1.14	7.55	1.19
B8R12P1c	115	1	Qtz-Ec	60.4	47.29	111.80	16.41	78.82	19.23	8.14	18.87	2.55	13.2	2.55	7.30	1.00	6.59	1.03
B149R127P7	347	1	Rt-Ec	44.8	62.49	143.40	17.58	72.89	15.97	4.91	14.78	2.12	9.94	1.80	4.52	0.53	3.16	0.46
B261R222P1a	532	2	Rt-Ec	27.60	5.90	12.80	1.87	9.27	3.06	1.61	4.71	0.90	6.24	1.36	3.77	0.53	3.29	0.50
B262R222P1f	533	2	Rt-Ec	56.20	24.70	64.20	10.30	54.50	15.00	6.20	16.70	2.48	13.80	2.71	6.86	0.84	4.79	0.67
B289R235P1m	576	2	Rt-Ec	8.84	0.15	0.49	0.13	1.37	1.38	1.00	1.99	0.34	2.05	0.42	1.09	0.15	0.87	0.12
B308R254P2	613	3	Mg-Ec	11.80	33.80	70.20	8.73	34.30	6.01	1.48	4.29	0.59	3.01	0.54	1.41	0.18	1.10	0.15
B353R283P1g	685	3	Mg-Ec	5.32	1.77	4.79	0.72	3.49	1.14	0.69	1.49	0.23	1.37	0.28	0.71	0.10	0.65	0.10
B355R283P1o	688	4	Phn-Ec	4.17	6.23	11.50	1.40	5.93	1.51	0.86	1.45	0.19	1.06	0.20	0.55	0.08	0.49	0.07
B382R300P2aL	731	4	Nor-Ec	19.70	1.36	3.69	0.64	3.73	2.13	1.16	3.43	0.66	4.21	0.86	2.38	0.33	2.11	0.31
B552R399P1l	1,003	4	Nor-Ec	26.20	10.50	23.40	3.09	13.90	3.32	1.54	4.26	0.75	4.88	1.03	2.91	0.41	2.67	0.40
B1033R645P5	1,964	6	Phn-Ec	12.3	7.10	15.2	2.61	11.1	2.40	0.98	2.82	0.31	2.51	0.50	1.43	0.22	1.35	0.20
B107R98P6k	282	1	Sch	49.6	21.93	54.36	7.59	34.79	8.54	3.38	8.73	1.57	9.34	2.03	6.26	0.93	6.42	1.01
B163R140P1mL	371	1	Sch	107	37.66	96.71	15.16	69.15	18.95	5.24	21.01	3.55	21.0	4.20	11.8	1.61	10.0	1.45
B488R369P1h	902	4	Pgn	36.0	27.3	47.4	6.3	24.4	5.0	1.8	6.0	1.0	6.5	1.4	4.1	0.6	3.9	0.6
B506R378P1d	930	4	Pgn	8.2	82.4	123.0	16.5	56.3	8.7	2.0	7.0	0.7	2.5	0.4	0.9	0.1	0.6	0.1
B578R418P1	1,050	4	Pgn	54.9	40.6	110.0	18.6	82.5	16.1	3.5	13.9	1.8	10.1	1.9	5.3	0.8	5.3	0.8
B616R436P1aL	1,109	4	Pgn	25.5	59.2	100.0	10.4	34.4	5.3	0.9	4.3	0.7	4.1	0.9	2.9	0.5	3.2	0.5
B743R516P12L	1,385	5	Ogn	120.0	91.1	154.0	18.9	70.3	13.7	0.9	13.6	2.5	16.5	3.6	11.5	1.8	11.8	1.7
B765R532P40	1,447	5	Ogn	64.4	64.6	129.0	14.3	52.2	10.9	0.8	9.0	1.8	10.9	2.3	6.8	1.0	6.2	0.9
B786R546P10a	1,504	5	Ogn	90.0	57.9	102.0	13.3	47.3	10.9	0.4	11.0	2.1	13.6	3.0	8.6	1.3	8.8	1.3

incompatible elements (e.g., Rb, Ba, Th) and Nb, whereas a few show slight enrichment in these elements (Fig. 11e). They have variable REE patterns, such as flat, LREE enrichment and depletion (Fig. 12e). Eclogites from units 4, 5 and 6 show comparable trace element patterns that are characterized by variable enrichment in large-ion lithophile elements (Rb, Ba, K), but negative Th, U, Nb, Ta and Ti anomalies (Fig. 11f, g), implying a crustal origin. Most eclogites have flat and fractionated REE patterns with LREE enrichment; some have slightly positive Eu anomalies (Fig. 12f, g).

Discussion

UHP metamorphic *P–T* conditions

Petrographic investigations demonstrate that the early UHP assemblages in gneiss and schist occur only as minor relics or as isolate inclusions in zircons, due to extensive retrograde metamorphism. Therefore, it is difficult to estimate *P–T* conditions of UHP metamorphism for these rocks. In this paper, our main efforts are focused on eclogites.

Metamorphic temperatures of eclogites were estimated from Fe^{2+}–Mg partitioning (K_D) between coexisting garnet and omphacite. Because most eclogitic garnets have very low Fe_2O_3 contents, total Fe of garnets is taken as Fe^{2+}. Therefore, the K_D value mainly depends on Fe_2O_3 contents of the coexisting clinopyroxene. Two methods are used to estimate Fe_2O_3 of clinopyroxene. One is to assume Fe^{3+} to be equal to Na–Al^{VI}, and the other is to estimate Fe^{3+} on the basis of stoichiometric charge balance. In order to investigate the possible effects of whole-rock compositions on temperature estimates, we compare the validity of the different geothermometers and evaluate the two methods of Fe^{3+} estimation.

Metamorphic temperatures of eclogites were calculated using the two methods of Fe^{3+} estimates and five calibrations of Fe^{2+}–Mg exchange thermometers (Ellis and Green 1979; Powell 1985; Krogh 1988; Yang 1994; Ravna 2000). Most estimates derived from the thermometer of Krogh (1988) are close to the mean values of the other four calibrations. Temperature estimates derived from the different methods of Fe^{3+} calculation do not agree in most cases, the largest difference is up to 124°C (sample B319R262P16A) (Table 5; Fig. 13a). However, consistent *T* estimates were obtained for Al-rich phengite- and kyanite-bearing eclogites. Using the calibration of Ravna (2000), even larger temperature

differences up to 160°C (sample B157R135P7L) are obtained for most samples except for Al-rich eclogites (Table 5; Fig. 13b). Figure 13 demonstrates that the estimated temperatures have negative correlations with TFeO contents of whole rocks. For Fe-rich eclogites (TFeO > 13%), most temperature estimates are less than 700°C, and even as low as 600°C, which are less than the peak-UHP metamorphic temperatures (700–800°C) given by most previous investigators for Sulu eclogites (e.g., Hirajima et al. 1990; Enami et al. 1993, 2000; Zhang et al. 1994, 1995a, 2000b, 2003; You et al. 1996; Cong et al. 1996). In conclusion it is likely that for Fe-rich eclogites all garnet–clinopyroxene Fe^{2+}–Mg exchange geothermometers do not yield reasonable temperatures.

According to Ravna and Milke (2001), reliable equilibrium pressures and temperatures for phengite- and kyanite-bearing eclogites can be calculated through three equilibrium reactions: (1) Prp + 2Grs + 3Cel = 6Di + 3Ms, (2) Prp + Grs + 2Cs = 3Di + 2Ky, (3) Alm + Grs + 2Cs = 3Hd + 2Ky, and the Fe^{2+}–Mg exchange thermometer between coexisting garnet and omphacite. As shown in Fig. 14 and Table 5, temperatures of 678–816°C and pressures of 3.1–4.4 GPa are obtained using the geothermobarometry of phengite–kyanite–coesite eclogites (Ravna and Milke 2001) when assuming that Fe^{3+} in omphacite equals to $Na–Al^{VI}$.

Although *P–T* estimates for eclogites fall in the UHP metamorphic field above the stability of coesite and even diamond, the largest pressure and temperature differences for eclogite are up to 1.3 GPa and 138°C. If these *P–T* estimates reflect the peak-metamorphic conditions, the UHP rocks must have been subducted to different depths, with the largest depth difference of up to 40 km; subsequently the UHP rocks formed at different depths must be tectonically transported to their present location. Alternatively, the lower *P–T* estimates do not represent peak-metamorphic conditions. Because of compositional re-equilibrations among garnet, clinopyroxene and phengite during the earliest stage of retrogression of UHP rocks, lower *P–T* conditions are recorded by these minerals. The recognition of retrograde growth zoning in garnet and diffusion zoning in clinopyroxene and phengite suggest that such readjustment is the main cause for the low *P–T* estimates (Zhang et al. 2005a, c).

Protoliths of the various rocks

As already discussed, eclogites from the CCSD-MH show characteristic features of metamorphosed magmatic rocks formed by extensive fractional crystallization in continental environments. This conclusion is supported by the following evidence: (1) eclogites show comparable compositional ranges to typical continental intrusions, such as the East Greenland and North Atlantic Province plutonic rocks, and resemble continental basalts in trace element and REE patterns; (2) Rt eclogites have the same chemical characteristics as Fe–Ti gabbros from typical layered mafic–ultramafic intrusions formed in continental environment, and metamorphosed Fe–Ti gabbros from continental orogenic belts (also see following section); (3) eclogites have low Mg numbers (mostly < 50%), suggesting that they are not derived from primitive melts; (4) the majority of the eclogites have Ti/V ratios between 20 and 50 and Y/Nb > 4, corresponding to continental basalts as suggested for Dabie-Sulu eclogites by Jahn (1998); (5) the correlations among major and trace elements suggest that eclogites have experienced variable degrees of fractional crystallization; (6) zircons from eclogites have well developed core–rim structures, i.e. an inherited magmatic core and a UHP metamorphic overgrowth rim (Zhang et al. 2006). Moreover, the cores show broad-concentric oscillatory or broad-band zoning patterns, which are usually observed in magmatic zircons from mafic intrusions (Rubatto and Scambelluri 2003). In addition, these features are also consistent with Sr–Nd–Pb isotopic results (Xiao et al., unpublished data), which indicate crustal signatures.

Eclogites and garnet peridotites in units 1, 2 and 3 are believed to belong to a single intrusive body, as supported by surface mapping and subsurface tectonic relationships (Xu et al. 1998, 2004; Zhang et al. 2000b, 2003). They represent products of variable degrees of fractional crystallization of basaltic melt. The protoliths of Rt eclogites from units 1 and 2 are Fe–Ti gabbros as they have the same chemical compositions as typical Fe–Ti gabbros and metamorphosed Fe–Ti gabbros, such as (1) lower SiO_2 contents than normal gabbros. In most cases, SiO_2 contents of Fe–Ti gabbros are less than 45%, or even as low as 30% due to abundant magnetite (up to 10–30% by volume), and in some cases due to abundant apatite (up to 15%) (Wager and Brown 1968; Arnason et al. 1997; Brandriss and Bird 1999; Barr et al. 2000). (2) They have relatively high FeO, TiO_2, P_2O_5 and V contents and relative low Zr, Nb and Ta contents (Table 4; Figs. 7, 8, 10). In most cases, TiO_2 versus SiO_2 shows a negative correlation (Fig. 10), whereas TiO_2 versus TFeO a positive correlation. Moreover, they are characterized by a decoupling of Ti from other high-field strength elements (HFSE), which is in contrast to modern

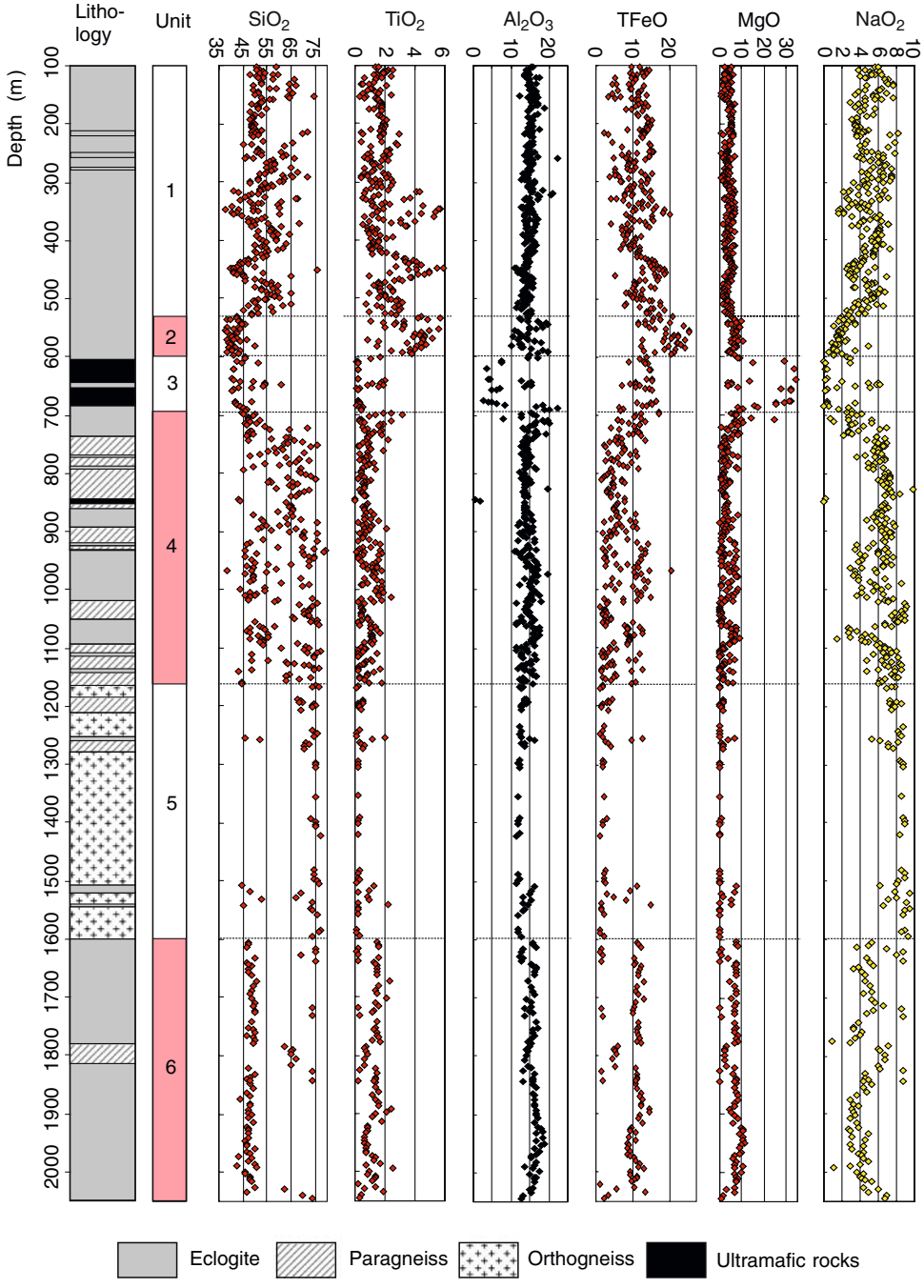

Fig. 7 Major element profiles of the CCSD-MH (100–2,050 m)

continental flood basalts in which Nb, Ta and Zr correlate positively with TiO_2. Wiebe (1993) concluded that FeO, TiO_2 P_2O_5 and V contents of layered gabbros will increase with the incoming of cumulus magnetite, ilmenite and apatite. Liu et al. (2005b) argued that magnetite is able to fractionate HFSE from Ti due to Ti and V partition coefficients between magnetite and mafic melt being > 1, whereas Nd, Zr, Ta partition coefficients are < 1; (3) they have relatively low REE concentrations, and show nearly flat and slightly LREE-depleted, but highly positive Eu anomaly REE patterns (see Fig. 12d) implying an accumulation of abundant plagioclases (e.g., Morrison et al. 1986; Arnason et al. 1997; Barandriss and Bird 1999; Cox et al. 1999).

Most layered intrusions are the products of multiple injections of magma and interval fractional crystallization. Therefore, they commonly have composite components and macrorhythmic layering (Parsons et al. 1986; Morrison et al. 1986; Wiebe 1993; Arnason et al. 1997). Cyclic and alternate occurrences of Qtz- and Rt-rich eclogite layers in units 1 and 2

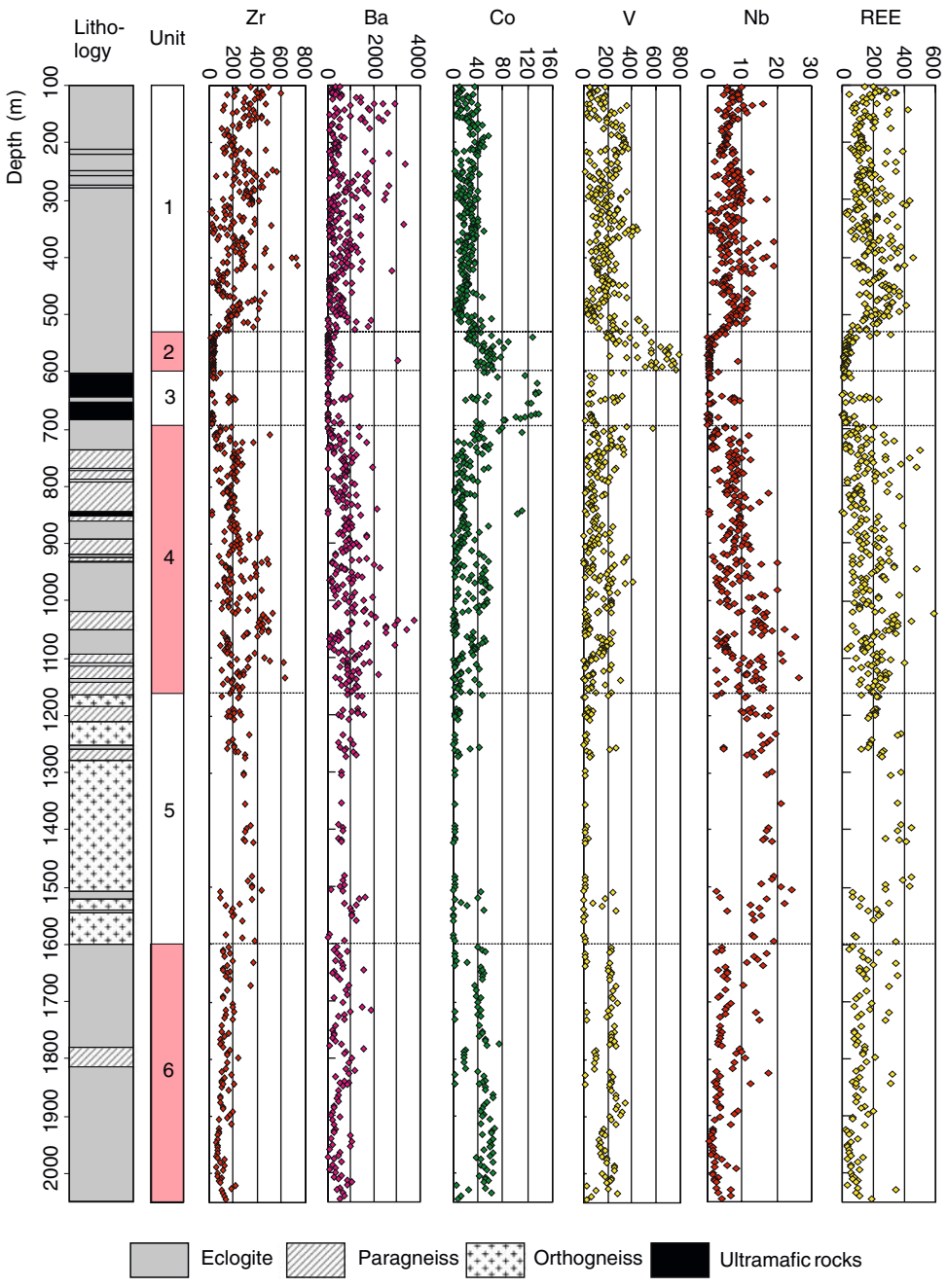

Fig. 8 Trace element profiles of the CCSD-MH (100–2,050 m)

should be reflecting the original rhythmic structure of the layered gabbro. Therefore, we consider that extensive fractional crystallization and multiple injections of more primitive melt in an evolved basaltic magma chamber should be the mechanism of Ti enrichment and the repeated occurrence of Ti-(Fe)-rich eclogitic layers.

Layered gabbro intrusions commonly have a base of ultramafic cumulates that were formed at the early stage of fractionation crystallization of basaltic melt (Wager and Brown 1968; Parsons et al. 1986; Morrison et al. 1986; Mathison 1987; Wiebe 1993; Arnason et al. 1997; Brandriss and Bird 1999). The garnet peridotite layer of unit 3 can be considered as the base of eclogite layers of units 1 and 2 as they are closely associated in space. Moreover, the ultramafic rocks are of crustal origin, as supported by oxygen isotopic evidence. Garnets, olivine and pyroxenes from ultramafic rocks have slightly lower oxygen isotopic values than normal mantle rocks (Li et al. 2006), implying that the peridotitic protoliths have been altered by the interactions with meteoric waters (Zhang et al. 2000a, 2005d; Xiao et al. 2000, 2002, 2006; Rumble et al. 2002). We therefore conclude that the garnet peridotites and

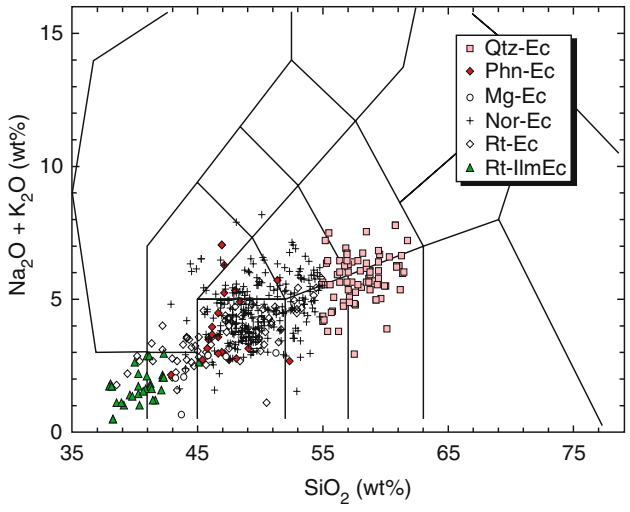

Fig. 9 $Na_2O + K_2O$ versus SiO_2 (TAS) diagram for various eclogites (classification after Middlemost 1994)

eclogites form these units and are the base and the main body of a layered mafic–ultramafic intrusion, respectively.

Rocks in unit 4 and 6 are frequently intercalated paragneisses and eclogites. As mentioned above, the eclogites are characterized by enrichments in LILE and negative Nb, Ta and Ti anomalies (Fig. 11f, g), which are typical features of continental rift basalt (Pearce and Peate 1995). Furthermore, there is no Eu anomaly in these eclogites (Fig. 12f, g), indicating that they cannot be explained in terms of different degrees of fractional crystallization. The interlayered paragneisses, on the other hand, have overall silicic compositions (65–75% SiO_2), low CaO (1–4%), relatively high Na_2O (3–8%), abundance and pronounced LREE enrichment REE patterns that are similar to continental sediments (Fig. 12a). This is consistent with the conclusion of Liu et al. (2001) and Zhang et al. (2003) that the protoliths of Sulu paragneisses are sedimentary rocks of relatively high maturity and continental affinity. In addition, zircons from paragneisses have no inherited magmatic core, but contain UHP metamorphic mineral inclusions, suggesting that they were formed during UHP metamorphism (Zhang et al. 2006), whereas zircons from eclogites often have a small magmatic core, typical for basaltic zircons, and a variable rim of metamorphic overgrowth. We suggest that eclogites and paragneisses from units 4 and 6 represent a meta-supracrustal rock series consisting of continental basalts and sediments.

Majority of the rocks in unit 5 are orthogneisses, as shown by Liu et al. (2004, 2005a). They have 70–80% SiO_2, 11–13% Al_2O_3, 7–9% CaO, 7–9% $Na_2O + K_2O$ (mostly $Na_2O < K_2O$), 0.2–2% TiO_2 (mostly < 1%), 0.2–1.4 total Fe oxide (mostly between 0.5 and 1%). They show the highest abundance of LILE compared to all other rock types. Their incompatible element

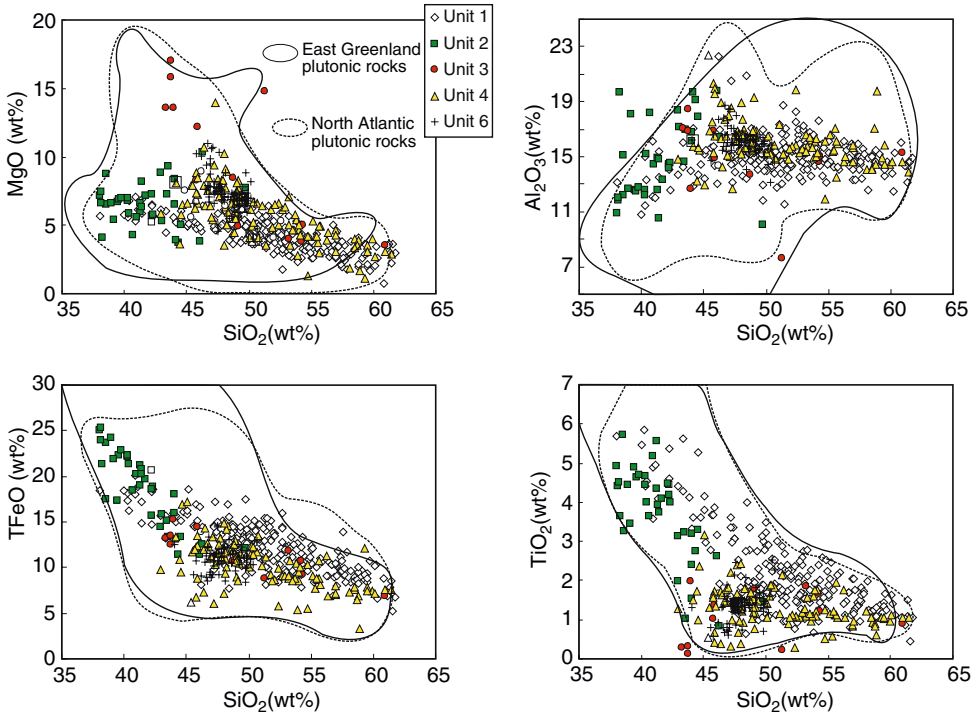

Fig. 10 Major elements versus SiO_2 diagram for eclogites from various units. Data of the East Greenland plutonic rocks and the North Atlantic plutonic rocks are from http://georoc.mpch-mainz.gwdg.de/georoc/

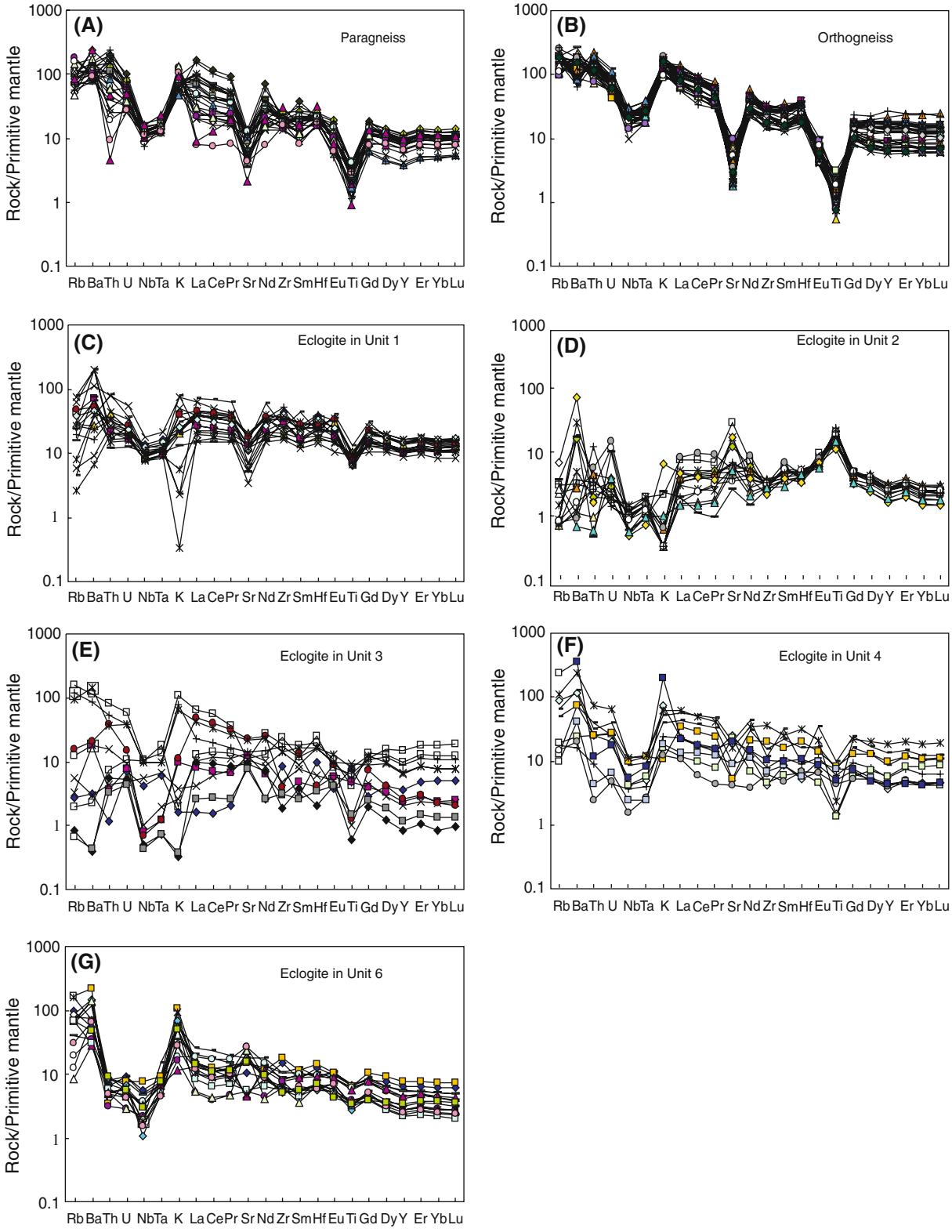

Fig. 11 Primary mantle normalized trace element patterns for various UHP rocks

patterns show strongly negative Nb, Ta, Sr and Ti anomalies, but positive Th, K and Nd anomalies (Fig. 11b). These geochemical characteristics strongly indicate that their protoliths are granitic rocks. Furthermore, their systematic variation in HREE implies a fractional crystallization process (Fig. 12b).

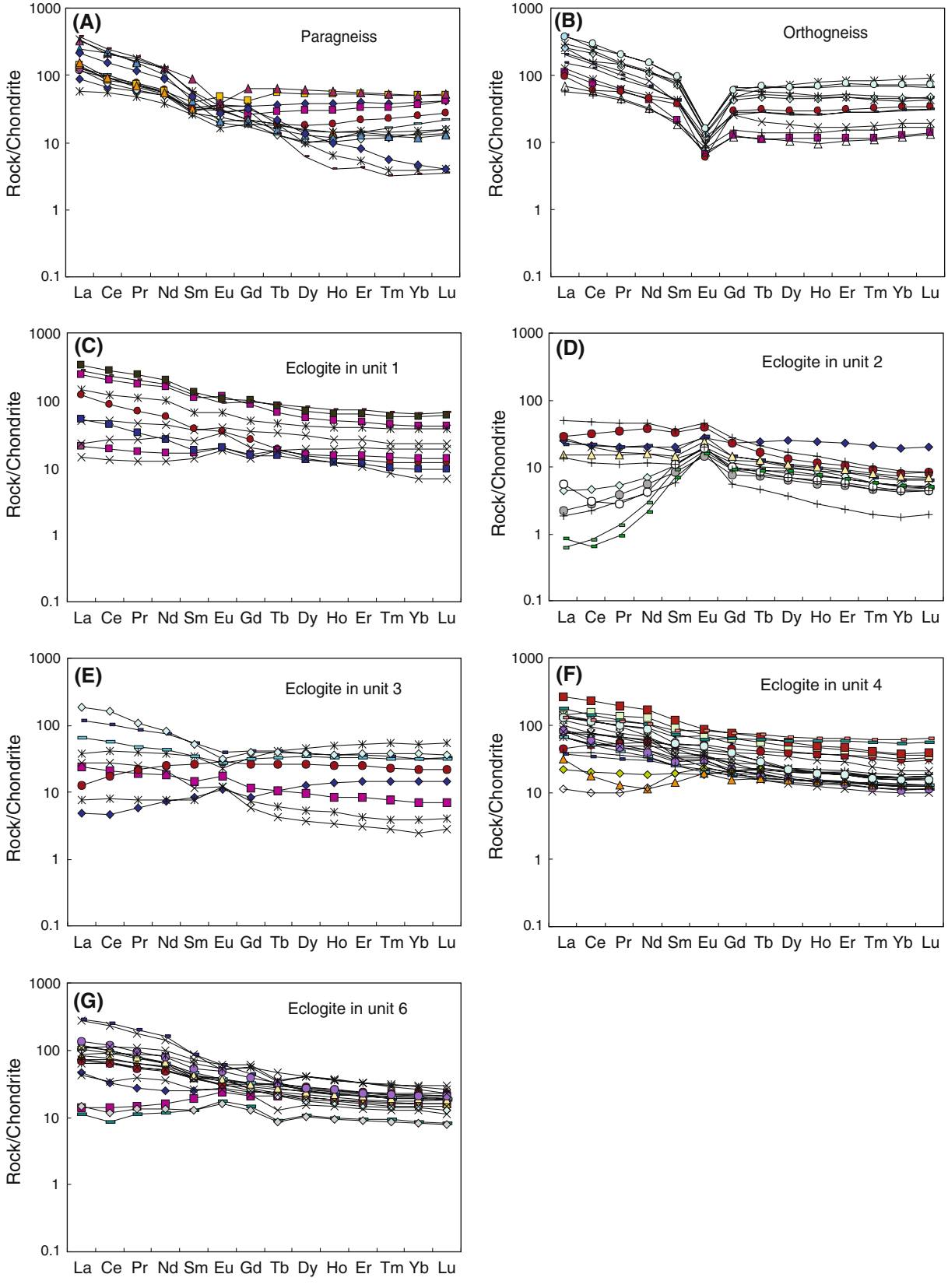

Fig. 12 Chondrite normalized REE patterns for various UHP rocks

Table 5 Metamorphic *P–T* estimates of various eclogite from the CCSD-MH

Sample	Depth (m)	Unit	Rock	*T*1 (*P* = 3.0 GPa)				*T*2	*P*
				K'88	R'00	K'88	R'00	R'01	
				Fe^{3+} = stoic.		Fe^{3+} = Na–Al		Fe^{3+} = Na–Al	
B1R1P1a	102	1	Qtz-Ec	760	770	737	750	815	4.3
B4R7P2e	109		Rt-Ec	630	670	588	625		
B8R12P1a	115		Qtz-Ec	734	755	682	700	728	3.7
B65R62P2a	215		Nor-Ec	730	684	696	685	731	4.0
B79R74P1d	235		Rt-Ec	608	608	637	685		
B125R110P1a	310		Qtz-Ec	694	686	676	675	700	3.7
B126R110P1dA	312		Nor-Ec	810	809	730	725	766	3.7
B129R112P1d	317		Rt-Ec	591	590	597	621		
B132R114P1a	320		Phn-Ec	739	766	755	755	798	3.7
B136R118P3d	325		Nor-Ec	820	815	759	748		
B149R127P7	347		Rt-Ec	738	821	658	712		
B153R131P1s	353		Rt-Ec	633	676	665	678		
B157R135P7L	360		Rt-Ec	555	576	629	736		
B187R167P1h	414		Qtz-Ec	769	790	678	698	760	4.3
B199R176P6i	433		Rt-Ec	697	727	605	628		
B200R177P1j	435		Rt-Ec	722	675	649	795	678	3.1
B209R186P1c	450		Rt-Ec	496	545	522	605		
B211R187P2a	453		Rt-Ec	586	640	563	615		
B214R190P1e	458		Rt-Ec	560	645	503	580		
B219R192P1i	465		Rt-Ec	741	745	662	665		
B247R210P2u	507		Rt-Ec	537	590	528	581		
B250R212P1cA	511		Rt-Ec	608	615	608	635		
B256R215P3jA	523		Qtz-Ec	683	675	629	655	682	3.6
B261R222P1a	532	2	Rt-Ec	570	590	583	615		
B262R222P1f	533		Rt-Ec	632	681	588	640		
B269R225P4m	544		Rt-Ec	764	756	802	845		
B287R235P1d	574		Rt-Ec	722	646	650	718		
B289R235P1m	576		Rt-Ec	722	706	713	700		
B301R246P1d	597		Rt-Ec	584	576	656	726		
B312R257P9a	618	3	Mg-Ec	657	680	629	661		
B319R262P16A	631		Mg-Ec	651	730	527	611		
B353R283P1d	685		Mg-Ec	566	566	523	517		
B355R283P1o-1	688	4	Phn-Ec	810	738	719	738	795	4.4
B355R283P1o-2	688		Phn-Ec	835	736	821	736	794	4.4
B358R285P1t	692		Rt-Ec	632	676	621	677		
B368R291P1g	710		Phn-Ec	763	702	763	702	727	3.4
B368R291P1g-2	710		Phn-Ec	738	680	755	701	716	3.7
B369R291P1k	711		Nor-Ec	815	758	693	758	816	3.9
B382R300P2aL	731		Nor-Ec	812	760	763	785		
B552R399P11	1,003		Nor-Ec	724	790	758	889		4.3
B926R613P12n	1,778	6	Nor-Ec	760	745	717	705		
B966R629P34q	1,855		Nor-Ec	728	715	733	745		
B992R636P48d	1,901		Nor-Ec	747	715	727	703	750	3.9
B1018R641P27	1,940		Phn-Ec	706	678	741	678	712	3.7
B1024R643P3c	1,951		Phn-Ec	774	690	774	690	756	4.2
B1033R645P5	1,964		Phn-Ec	772	716	772	716	742	3.7
B1040R646P5f	1,975		Nor-Ec	716	678	728	730	775	3.8

*T*1 are estimated using the calibrations of Krogh (1988) and Ravna (2000), assumed *P* = 3.0 GPa, and Fe^{3+} in Cpx are recalculated by the charge balance or equal to Na–Al; *T*2 and *P* are estimated by the geothermobarometry of phengite–kyanite–coesite eclogites (Ravna and Milke 2001), and Fe^{3+} = Na–Al.

Zircons from orthogneisses form euhedral long prismatic crystals, with oscillatory zonations formed by magmatic crystallization, indicating that their protoliths were derived from a granitic intrusion (Zhang et al. 2006).

Conclusions

1. The CCSD-MH has collected many typical UHP metamorphic rocks, including eclogite, orthogneiss, paragneiss, ultramafic rock and minor schist.

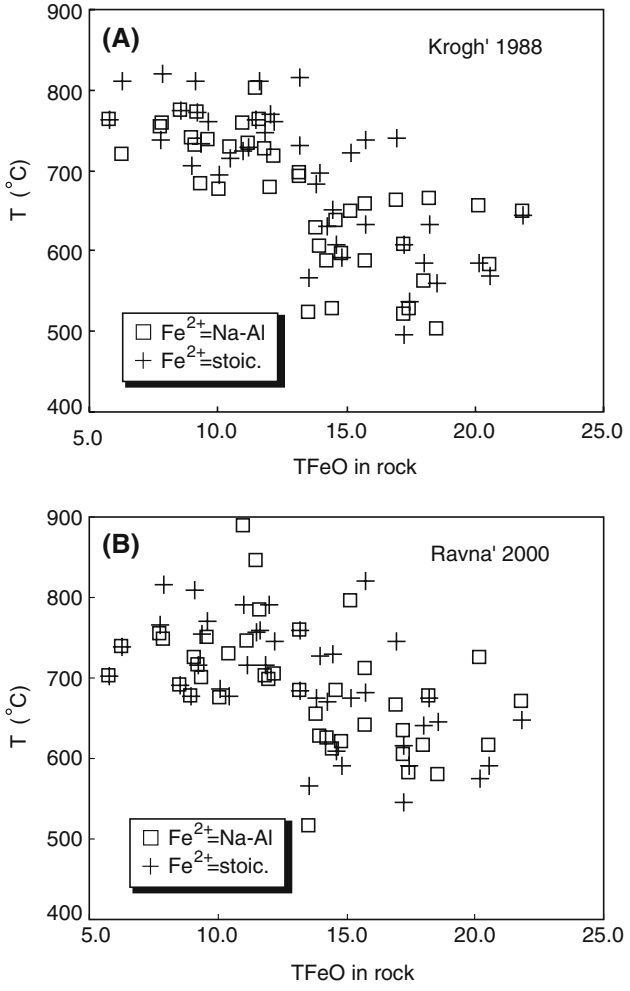

Fig. 13 Relationship between temperature estimates and total FeO contents of the eclogites. Temperature values are estimated by the calibration of Krogh (1988) (**a**) and Ravna (2000) (**b**) at an assumed pressure of 3.0 GPa. Fe^{3+} in clinopyroxene is adjusted by Fe^{3+} = Na–Al or by stoichiometric charge balance, respectively

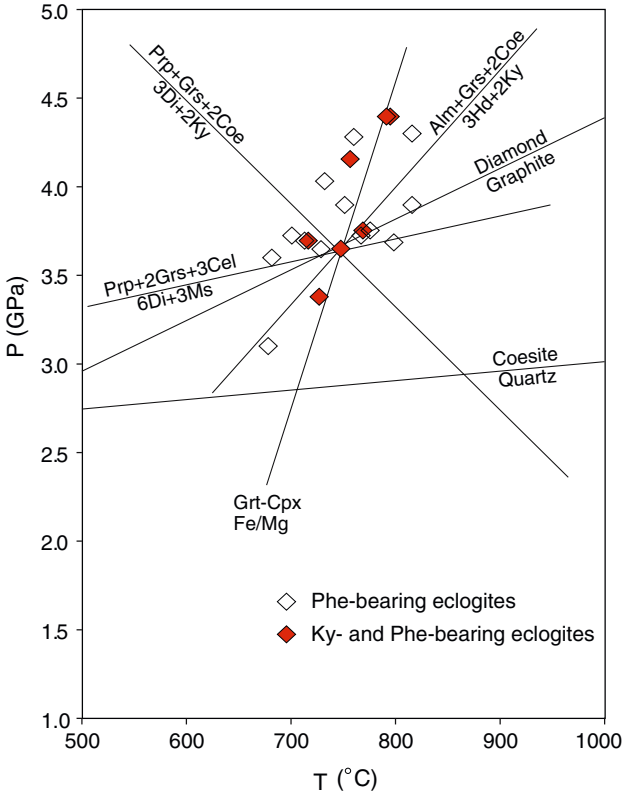

Fig. 14 Estimated *P–T* conditions of kyanite- and/or phengite-bearing eclogites from the CCSD-MH, showing equilibration reaction curves of a representative phengite–kyanite eclogite (R1033R645P5) calculated by the geothermobarometry of Ravna and Milke (2001). The Fe–Mg exchange thermometer between garnet and omphacite is based on the calibration of Ravna (2000) and Fe^{3+} in omphacite equal to Na–Al. The coesite–quartz and diamond–graphite transformation boundaries are after Bohlen and Boettcher (1982) and Kennedy and Kennedy (1976), respectively

Eclogites show a UHP mineral assemblage including garnet, omphacite, coesite, rutile, phengite, kyanite, zoisite, apatite and zircon. Country gneiss and schist consist of amphibolite-facies minerals. Zircons containing coesite along with garnet, omphacite, phengite, rutile and apatite inclusions in all country rocks indicate that these rocks together with the eclogites have been subjected to early UHP metamorphism before amphibolite-facies retrogression. Combining the data from the main hole with other shallow holes and surface outcrops from Sulu area, we suggest that a huge supracrustal rock slab (> 50 km long × 100 km wide × 5 km depth) was subducted to a depth > 100 km, and then exhumed to the surface.

2. Geochemical characteristics show that eclogites and orthogneisses from CCSD-MH have affinities to continental intrusive rocks. Protoliths of the eclogites and ultramafic rocks from units 1, 2 and 3 are a layered mafic to ultramafic intrusive body which was formed by fractional crystallization of a basaltic magma at crustal depths. Eclogites from units 4 and 6 together with interlayered paragneisses are meta-supracrustal volcanic and sediment series; orthogneisses from unit 5 have a granitic protolith.
3. Equilibrium temperatures of 678–816°C and pressures of 3.1–4.4 GPa are estimated for the phengite- and kyanite-bearing eclogites. Temperatures of formation for the FeO-rich eclogites (TFeO > 13%) cannot be estimated by available garnet–clinopyroxene Fe–Mg exchange thermometers. Recognition of a retrograde compositional zoning of garnet, omphacite and phengite suggests that peak-metamorphic conditions of some UHP rocks

have not been well preserved due to re-equilibration during early retrograde metamorphism.

4. FeO, MgO and Al_2O_3 contents of eclogitic garnets and Na_2O, FeO and MgO contents of eclogitic omphacites show positive correlations with whole-rock compositions. However, CaO of garnets, CaO and Al_2O_3 of omphacites and SiO_2 of phengites are not related to those of the whole-rocks, suggesting that compositions of these phases were controlled mainly by the metamorphic temperature and/or pressure of the host rocks.

Acknowledgments This work was supported by the Major State Basic Research Development Program (2003CB716501), the National Natural Scientific Foundation of China (40399142 and 40472036), the National Science Foundation of Germany (DFG, Ho 375/22) and the US National Science Foundation (EAR 0003355). We sincerely thank Profs. Xu Zhiqin, Yang Jingsui, Liu Fulai, Shen Kun, You Zhendong, Jin Zhenmin, Gao Yongjun and the scientists from the Geoscience Centre of Göttingen for help during various stages of the research. We thank Prof. Pascal Philippot, an anonymous reviewer, and Borming Jahn for their critical review of the original manuscript.

References

Armstrong JT (1991) Quantitative elemental analysis of individual microparticles with electron beam instruments. In: Heinrich KFJ, Newbury DE (eds) Electron probe quantization. Plenum Press, New York, pp 261–285

Arnason JG, Bird DK, Bernstein S, Rose NM, Manning CE (1997) Petrology and geochemistry of the Kruuse Fjod gabbro complex, east Greenland. Geol Mag 134:67–89

Barr SM, Hamilton MA, White CE, Samson SD (2000) A Late Neoproterozoic age for the Caledonia Mountain Pluton, a high Ti–V layered gabbro in the Caledonia (Avalon) terrane, southern New Brunswick. Atl Geol 36:157–166

Bohlen SR, Boettcher AL (1982) The quartz-coesite transformations: a pressure determination and the effects of other composition. J Geophys Res 87:7073–7078

Brandriss M, Bird D (1999) Effects of H_2O on phase relations during crystallization of gabbros in the Kap Edvard Holm complex, east Greenland. J Petrol 40:1037–1064

Cong BL, Wang QC (1996) A review on researches of UHPM rocks in the Dabieshan-Sulu Region. In: Cong BL (ed) Ultrahigh-pressure metamorphic rocks in the Dabieshan-Sulu region of China. Science Press, Beijing, pp 1–170

Cox RA, Indares A (1999) Transformation Fe–Ti gabbro to coronite, eclogite and amphibolite in the Baie du Nord segment, Manicouagan Imbricate Zone, eastern Grenville Province. J Metamorph Geol 17:537–555

Cox RA, Dunning GR, Indares A (1998) Petrology and U-Pb geochronology of mafic, high-pressure, metamorphic coronites from the Tshenukutish domain, eastern Grenville Province. Precambrian Res 90:59–83

Ellis DJ, Green DH (1979) An experimental study of the effect of Ca upon garnet–clinopyroxene Fe–Mg exchange equilibrium. Contrib Mineral Petrol 71:13–22

Enami M, Nagasaki A (2000) Prograde *P–T* path of kyanite eclogites from Junan in the Sulu ultrahigh-pressure province, eastern China. Island Arc 8:495–474

Enami M, Zang Q, Yin Y (1993) High-pressure eclogites in northern Jiangsu–southern Sangdong province, eastern China. J Metamorph Geol 11:589–603

Hirajima T, Ishiwateri A, Cong B, Zhang R, Banno S, Nozaka T (1990) Identification of coesite in Mengzhong eclogite from Donghai county, northeastern Jiangsu Province, China. Mineral Mag 54:579–584

Jahn BM (1998) Geochemical and isotopic characteristics of UHP eclogites and ultramafic rocks of the Dabie orogen. In: Hacker BR, Liou JG (eds) When continents collide: geochemistry of ultrahigh-pressure rocks. Kluwer, Dordrecht, pp 203–239

Kennedy CA, Kennedy GC (1976) The equilibrium boundary between graphite and diamond. J Geophys Res 81:2467–2470

Kretz R (1983) Symbols for rock-forming minerals. Am Mineral 68:277–279

Krogh E (1988) The garnet–clinopyroxene Fe–Mg geothermometer—reinterpretation of existing experimental data. Contrib Mineral Petrol 99:44–48

Li TF, Yang JS, Rumble D (2006) Magmatic ultramafic rock in Sulu ultrahigh pressure metamorphic belt: depleted oxygen isotope evidence from main hole of Chinese Continental Scientific Drilling Project. Acta Petrol Sin (in press)

Liou JG, Banno S, Ernst WG (1995) Ultrahigh-pressure metamorphism and tectonics. Island Arc 4:233–239

Liou JG, Zhang RY, Ernst WG, Liu J, McLimans R (1998) Mineral parageneses in the Piampaludo eclogitic body, Gruppo di Voltri, Western Ligurian Alps. Schweiz Mineral Petrogr Mitt 78:317–335

Liu FL, Xu ZQ, Katayama I, Yang JS, Maruyama S, Liou JG (2001) Mineral inclusions in zircon of para- and orthogneiss from pre-pilot drillhole CCSD-PP1, Chinese continental scientific drilling project. Lithos 59:199–215

Liu FL, Xu ZQ, Xue HM (2004) Tracing the protolith, UHP metamorphism, and exhumation ages of orthogneiss from the SW Sulu terrane (eastern China): SHRIMP U–Pb dating of mineral inclusion-bearing zircons. Lithos 78:411–429

Liu FL, Xu ZQ, Xue HM, Meng FC (2005a) Ultrahigh-pressure mineral inclusions preserved in zircons separated from eclogite and its country-rocks in the main drill hole of Chinese Continental Scientific Drilling Project (0–4500 m). Acta Petrol Sin 21:277–292

Liu YS, Zhang ZM, Lee CT, Gao S (2005b) Decoupled high-Ti from low-Nb (Zr) of eclogites from the CCSD: implications for magnetite fractional crystallization in basalt chamber. Acta Petrol Sin 21:339–346

Mathison CI (1987) Cyclic units in the Somerset Dam layered gabbro intrusion, southeastern Queensland, Australia. Lithos 20:187–205

McBirney AR (1989) The Skaergaard layered series: I. Structure and average compositions. J Petrol 30:363–397

Middlemost EAK (1994) Naming materials in the magma/igneous rock system. Earth Sci Rev 37:215–224

Morrison DA, Maczuga DE, Phinney WC, Ashwal LD (1986) Stratigraphy and petrology of the Mulcahy Lake layered gabbro: an Archean intrusion in the Wabigoon Subprovince, Ontario. J Petrol 27:303–341

Parsons I, Brown W, Jacquemin H (1986) Mineral chemistry and crystallization conditions of the Mboutou layered gabbro-syenite-granite complex, north Cameroon. J Petrol 27:1305–1329

Pearce JA, Peate DW (1995) Tectonic implications of the composition of volcanic arc magmas. Annu Rev Earth Planet Sci 23:251–285

Powell R (1985) Regression diagnostic and robust regression in geothermometer/geobarometer calibration: the garnet–clinopyroxene geothermometer revisited. J Metamorph Geol 3:231–243

Ravna EK (2000) The garnet–clinopyroxene Fe^{2+}–Mg geothermometer: an updata calibration. J Metamorph Geol 18:211–219

Ravna K, Milke PT (2001) Geothermobarometry of phengite-kyanite-quartz/coesite eclogites. In: Eleventh annual V. M. Goldschmidt conference, Hot Springs, Virginia, p 3145

Rubatto D, Scambelluri M (2003) U–Pb dating of magmatic zircon and metamorphic baddeleyite in the Ligurian eclogites (Voltri Massif, Western Alps). Contrib Mineral Petrol 146:341–355

Rumble D, Giorgis D, Ireland T, Zhang ZM, Xu HF, Yui TF, Yang JS, Xu ZQ, Liou JG (2002) Low ^{18}O zircons, U–Pb dating, and the Qinglongshan oxygen and hydrogen isotope anomaly near Donghai in Jiangsu Province, China. Geochim Cosmochim Acta 66:2299–2306

Wager RL, Brown GM (1968) Layered igneous rocks. W.H. Freeman, San Francisco

Wallis S, Enami M, Banno S (1999) The Sulu UHP terrane: a review of the petrology and structural geology. Int Geol Rev 41:906–920

Wiebe RA (1993) The Pleasant Bay layered gabbro-diorite, Coastal Maine: ponding and crystallization of basaltic injections into a silicic magma chamber. J Petrol 34:461–489

Xiao YL, Hoefs J, Alfons M, van den Kerkhof AM, Fiebig J, Zheng YF (2000) Fluid history of UHP metamorphism in Dabie Shan, China: a fluid inclusion and oxygen isotope study on the coesite-bearing eclogite from Bixiling. Contrib Mineral Petrol 139:1–16

Xiao YL, Hoefs J, van den Kerkhof AM, Simon K, Fiebig J, Zheng YF (2002) Fluid evolution during HP and UHP metamorphism in DabieShan, China: constraints from mineral chemistry, fluid inclusions and stable isotopes. J Petrol 43:1505–1527

Xiao YL, Zhang ZM, Hoefs J, van den Kerkhof A (2006) Ultrahigh-pressure metamorphic rocks from the Chinese Continental Scientific Drilling Project—II. Oxygen isotope and fluid inclusion distributions through vertical sections. Contrib Mineral Petrol (this issue)

Xu ZQ, Yang WC, Zhang ZM, Yang TN (1998) Scientific significance and site-selection researches of the first Chinese Continental Scientific Deep Drillhole. Cont Dyn 3:1–13

Xu ZQ, Zhang ZM, Liu FL, Yang JS, Tang ZM, Cheng SZ, Cai YC, Li TF, Cheng FY (2004) The structure profile of 0–1,200 m in the main borehole, Chinese Continental Scientific Drilling and its preliminary deformation analysis. Acta Petrol Sin 20:53–72

Ya K, Yao YP, Katayama I, Cong BL, Wang QC, Maruyama S (2000) Large areal extent of ultrahigh-pressure metamorphism in the Sulu ultrahigh-pressure terrane of East China: new implications from coesite and omphacite inclusions in zircon of granitic gneiss. Lithos 52:157–164

Yang A (1994) A revision of the garnet–clinopyroxene Fe^{2+}–Mg exchange geothermometer. Contrib Mineral Petrol 115:467–473

Yang JJ (2003) Relict edenite in a garnet lherzolite from the Chinese Su-Lu UHP metamorphic terrane: implications for metamorphic history. Am Mineral 88:180–188

Yang JJ, Jahn BM (2000) Deep subduction of mantle-derived garnet peridotites from the Su-Lu UHPM terrane in China. J Metamorph Geol 18:167–180

You ZD, Han YJ, Yang WR, Zhang ZM, Wei BZ, Liu R (1996) The high-pressure and ultrahigh-pressure metamorphic belt in the east Qinling and Dabie Mountains, China. University of Geoscience Press, Wuhan

Zhang RY, Liou JG, Cong BL (1994) Petrogenesis of garnet-bearing ultramafic rocks and associated eclogites in the Su-Lu ultrahigh-pressure metamorphic terrane, China. J Metamorph Geol 12:169–186

Zhang RY, Hirajima T, Banno S, Cong BL, Liou JG (1995a) Petrology of ultrahigh-pressure rocks from the southern Sulu region, eastern China. J Metamorph Geol 13:659–675

Zhang RY, Liou JG, Cong BL (1995b) Talc-, magnesite- and Ti-clinohumite-bearing ultrahigh-pressure meta-mafic and ultramafic complex in the Dabie Mountains, China. J Petrol 36:1011–1037

Zhang RY, Liou JG, Yang J, Yui T (2000a) Petrochemical constraints for dual origin of garnet peridotites from the Dabie-Sulu UHP terrane, eastern-central China. J Metamorph Geol 18:149–166

Zhang ZM, Xu ZQ, Xu HF (2000b) Petrology of ultrahigh-pressure eclogite from the ZK703 drillhole in the Donghai, eastern China. Lithos 52:35–50

Zhang ZM, Xu ZQ, Xu HF (2003) Petrology of the non-mafic UHP metamorphic rocks from a drillhole in the Southern Sulu orogenic belt, eastern-central China. Acta Geol Sin 77:173–186

Zhang ZM, Xiao YL, Shen K, Gao YJ (2005a) Garnet growth compositional zonation and metamorphic *P–T* path of the ultrahigh-pressure eclogites from the Sulu orogenic belt, eastern central China. Acta Petrol Sin 21:809–818

Zhang ZM, Xiao YL, Liu FL, Liou JG, Hoefs J (2005b) Petrogenesis of UHP metamorphic rocks from Qinglongshan, Southern Sulu, East-Central China. Lithos 81:189–207

Zhang ZM, Zhang JF, You ZD, Shen K (2005c) Ultrahigh-pressure metamorphic *P–T–t* path of the Sulu orogenic belt, Eastern Central China. Acta Petrol Sin 21:257–270

Zhang ZM, Rumble D, Liou J, Xiao YL, Gao YJ (2005d) Oxygen isotope geochemistry of rocks from the Pre-Pilot Hole of the Chinese Continental Scientific Drilling Project (CCSD-PPH1). Am Mineral 90:857–863

Zhang ZM, Shen K, Xiao YL, Hoefs J, Liou JG, Xu ZQ (2006) Mineral and fluid inclusions in zircon of UHP metamorphic rocks from the CCSD-Main Drill Hole: a record of metamorphism and fluid activity. Lithos (in press)